AFRL-SN-RS-TR-2007-123
In-House Interim Technical Report
April 2007

PHOTONIC MODULATION USING BI-DIRECTIONAL DIAMOND SHAPED RING LASERS AT 1550 NM

APPROVED FOR PUBLIC RELEASE; DISTRIBUTION UNLIMITED.

STINFO COPY

AIR FORCE RESEARCH LABORATORY
SENSORS DIRECTORATE
ROME RESEARCH SITE
ROME, NEW YORK

NOTICE AND SIGNATURE PAGE

Using Government drawings, specifications, or other data included in this document for any purpose other than Government procurement does not in any way obligate the U.S. Government. The fact that the Government formulated or supplied the drawings, specifications, or other data does not license the holder or any other person or corporation; or convey any rights or permission to manufacture, use, or sell any patented invention that may relate to them.

This report was cleared for public release by the Air Force Research Laboratory Rome Research Site Public Affairs Office and is available to the general public, including foreign nationals. Copies may be obtained from the Defense Technical Information Center (DTIC) (http://www.dtic.mil).

AFRL-SN-RS-TR-2007-123 HAS BEEN REVIEWED AND IS APPROVED FOR PUBLICATION IN ACCORDANCE WITH ASSIGNED DISTRIBUTION STATEMENT.

FOR THE DIRECTOR:

/s/

JOHN C. RAMSEY
Acting Chief, Electro-Optics Branch

/s/

RICHARD G. SHAUGHNESSY
Chief, Rome Operations Site
Sensors Directorate

This report is published in the interest of scientific and technical information exchange, and its publication does not constitute the Government's approval or disapproval of its ideas or findings.

REPORT DOCUMENTATION PAGE

Form Approved
OMB No. 0704-0188

1. REPORT DATE *(DD-MM-YYYY)*	2. REPORT TYPE	3. DATES COVERED *(From - To)*
APR 2007	Interim	Nov 03 – Sep 06

4. TITLE AND SUBTITLE

PHOTONIC MODULATION USING BI-DIRECTIONAL DIAMOND SHAPED RING LASERS AT 1550 NM

5a. CONTRACT NUMBER
In-House

5b. GRANT NUMBER

5c. PROGRAM ELEMENT NUMBER
62204F

6. AUTHOR(S)

Rebecca Bussjager, Reinhard Erdmann, Vasilios Kovanis and Brian McKeon

5d. PROJECT NUMBER
SEMI

5e. TASK NUMBER
SN

5f. WORK UNIT NUMBER
01

7. PERFORMING ORGANIZATION NAME(S) AND ADDRESS(ES)
AFRL/SNDP
25 Electronic Pky
Rome NY 13441-4515

8. PERFORMING ORGANIZATION REPORT NUMBER

9. SPONSORING/MONITORING AGENCY NAME(S) AND ADDRESS(ES)

AFRL/SNDP
25 Electronic Pky
Rome NY 13441-4515

10. SPONSOR/MONITOR'S ACRONYM(S)

11. SPONSORING/MONITORING AGENCY REPORT NUMBER
AFRL-SN-RS-TR-2007-123

12. DISTRIBUTION AVAILABILITY STATEMENT
APPROVED FOR PUBLIC RELEASE; DISTRIBUTION UNLIMITED. PA# 07-207

13. SUPPLEMENTARY NOTES

14. ABSTRACT
The Air Force Research Laboratory/Sensors Directorate (AFRL/SNDP) Binoptics Corp, and Infotonics Technology Center worked collaboratively to characterize and eventually package diode-based, diamond-shaped cavity, ring lasers that operate at 1550 nm. The laser modes propagate bi-directionally; however, uniaxial propagation was induced by optical injection from a tunable diode laser. The four-port laser ring offers use as an indirect modulator, directional router, and optical logic devices. Each optical output retains the encoding with either positive or negative logic, which can be used for conventional digital signal processing or routing. Secondly, the two counter-propagating laser modes provide a direct means for realizing the Sagnac effect, which has been well established in gyro technology with gas and fiber lasers. The ring lasers described here offer an ultra compact geometry for potential laser gyro and inertial sensor applications. These devices are scaleable and monolithically integrable with many semi-conductor based components including optical amplifiers, photodiodes, and electro-absorption modulators (EAMs).

15. SUBJECT TERMS
Photonic ADC, O-E conversion, optical to electrical conversion, saturable absorber etalons, fiber laser, phase noise, timing jitter, electro-absorption modulators, EAMs

16. SECURITY CLASSIFICATION OF:			17. LIMITATION OF ABSTRACT	18. NUMBER OF PAGES	19a. NAME OF RESPONSIBLE PERSON
a. REPORT	b. ABSTRACT	c. THIS PAGE			Rebecca Bussjager
U	U	U	UL	60	19b. TELEPHONE NUMBER (*Include area code*)

Table of Contents

List of Figures

List of Tables

1.0 Introduction

The Air Force Research Laboratory/Sensors Directorate (AFRL/SNDP), Binoptics Corp., and Infotonics Technology Center worked collaboratively to characterize and eventually package diode based, diamond-shaped cavity, ring lasers that operate at 1550 nm. The laser modes propagate bi-directionally; however, uniaxial propagation was induced by optical injection from a tunable diode laser. When the input signal was time-encoded with an optical modulator, the encoding was transferred to both modes with an inverted time-intensity profile.

Initial investigations using diamond-shaped ring lasers occurred while SNDP researched photonic analog-to-digital conversion (ADC) techniques[1]. In military systems ADCs are an essential link between analog sensor systems such as RADAR, Electronic Warfare (EW), Signal Intelligence (SIGINT) and high-speed digital signal processing systems providing global awareness. Military utilization of high performance ADC technology is quite diverse, spanning a wide range of sample rates and bit resolution values. Commercial users benefit from high speed ADCs in the areas of high speed test equipment, medical imaging applications, telecommunications, and many more. Improvements in dynamic range, accuracy, stability, and resolution of any ADC will enhance the performance in commercial and military applications. Collaborative work with Binoptics opened the door for a potentially new high speed ADC architecture.

Additional applications become apparent:

1. The four-port laser ring offers use as an indirect modulator, directional router, and optical logic devices. The configuration transfers optical digitally encoded signals injected from an optical modulator to the four output ports. Each optical output retains the encoding with either positive or negative logic, which can be used for conventional digital signal processing or routing.
2. Secondly, the two counter-propagating laser modes provide a direct means for realizing the Sagnac effect, which has been well established in gyro technology with gas and fiber lasers. The ring lasers described here offer an ultra compact geometry for potential laser gyro and inertial sensor applications.
3. Another application is the extraction of weak signals from the noise floor. With stochastic resonance the addition of random noise to the spontaneous emission noise can significantly improve the signal-to-noise level of an externally modulated bi-stable nonlinear system relative to one with no injected noise. A ring laser port allows an all-optical approach to this, in contrast with prior ones[2] that were constrained to manipulate the electrical drive power.

These devices are scaleable and monolithically integrable with many semi-conductor based components including optical amplifiers, photodiodes, and electro-absorption modulators (EAMs).

The organization of this report begins with explanation of the semiconductor ring laser behavior in Chapter 2. Chapter 3 includes a discussion of proposed architectures in which diamond-shaped ring lasers may improve ADC performance.Chapter 4 presents experimental results for ring laser devices in continuous wave and pulsed formats ranging from 200 Hz to those exceeding 12 GHz. Characterization in terms of fidelity and extinction ratio, initially performed on device die, was later compared to the performance of fully packaged devices. A theoretical rate equation model is proposed in Chapter 5 to account for key aspects of the injected laser's behavior.

2.0 Semiconductor Ring Laser Behavior

Binoptics Corporation has demonstrated a new diamond shaped cavity configuration for semiconductor ring lasers that operate in the low loss fiber window near 1550 nm. Their novel etched facet technology allows facets to be defined through high precision photolithography, rather than traditional cleaving, offering flexibility and reproducibility in monolithic integration capability[3]. Depicted in Figure 1, the laser modes propagate bi-directionally, but the extent of uniaxial propagation can be influenced by implementing a mirror external to the cavity to suppress one of the modes or by laser injection at the ring's resonance. When light is injected in a particular fashion, the bidirectional ring laser is forced to propagate, or becomes a "slave" to injected light, in that direction.

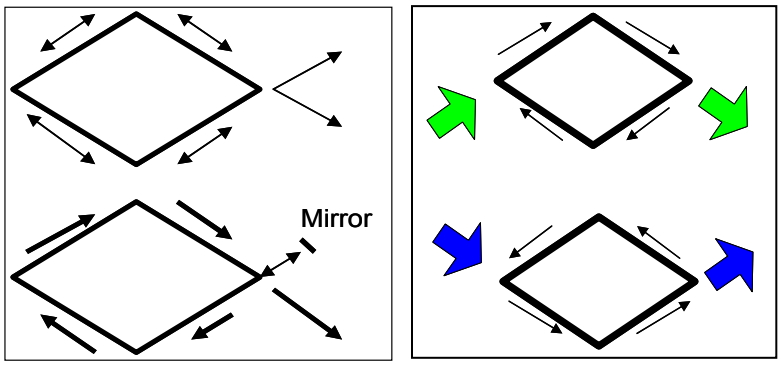

Figure 1. Diamond shaped ring laser operates bidirectionally and unidirectionally.

The unidirectional slave diamond ring can be thought of as a type of an inverter because when a beam is injected in the opposite direction with the proper optical conditions, the output will switch directions. This process happens extremely fast because carrier relaxation dynamics do not seem to come into play, as will be discussed further in Chapters 4 and 5. The diamond laser also becomes an inverter when configured with an external mirror. For example in Figure 2, the external facet is positioned to provide just enough feedback to cause the ring to operate in the clockwise (CW) state. Once light is introduced, it will cause the laser to switch from CW to counter-clockwise (CCW) operation. The laser returns to the CW state as soon as the injection light is extinguished. Figure 2 illustrates this and shows the truth table. The mirror forces the direction to be in the CW state allowing an output shown in the top. If a light beam is injected, indicated by the blue arrow, the rotation would switch to CCW rotation and there would be no output.

The focus of research reported here does not incorporate an external mirror, but it does investigate characteristics and applications of the switching behavior based on injection locking.

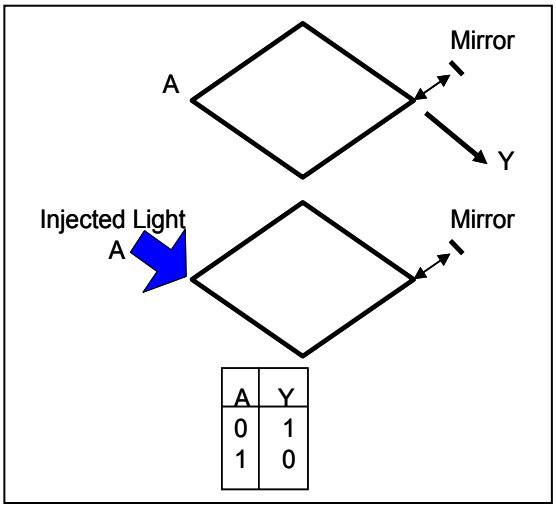

Figure 2. Ring laser operating as an optical inverter.

3.0 ADC Architectures

3.1 Flash ADC Using Binoptics' Devices

Photonic ADC architectures and the electronic versions face some of the same problems, such as size, complexity, weight and cost. Photonic architectures, though still in early stages, hold promise if the right components can be developed. In fact, Binoptics' integrated ring lasers, modulators, detectors and optical logic gates may prove to be critical to such a system.

Parallel flash converters are most appropriate for very high speed applications; however, they are typically limited to resolutions of 8-10 bits. A flash architecture, whether it is photonic or electronic, requires the input signal to be compared to a reference level in each of the 2^n-1 channels, and a block diagram is shown in Figure 3. This exponential complexity can place tight constraints on size, power and cost. Most importantly, the large number of channels requires small differences between reference levels, so this tolerance becomes the limiting factor in achieving high bit resolution. As a result, electronic flash ADCs traditionally are limited to applications requiring less than 8 bits with 10 bits on the "cutting edge". In addition implementing electronic flash ADCs at speeds greater than 1 GHz becomes difficult because high speed comparators are also a limiting factor due to the amount of time needed to sample the signal and reset the capacitor.

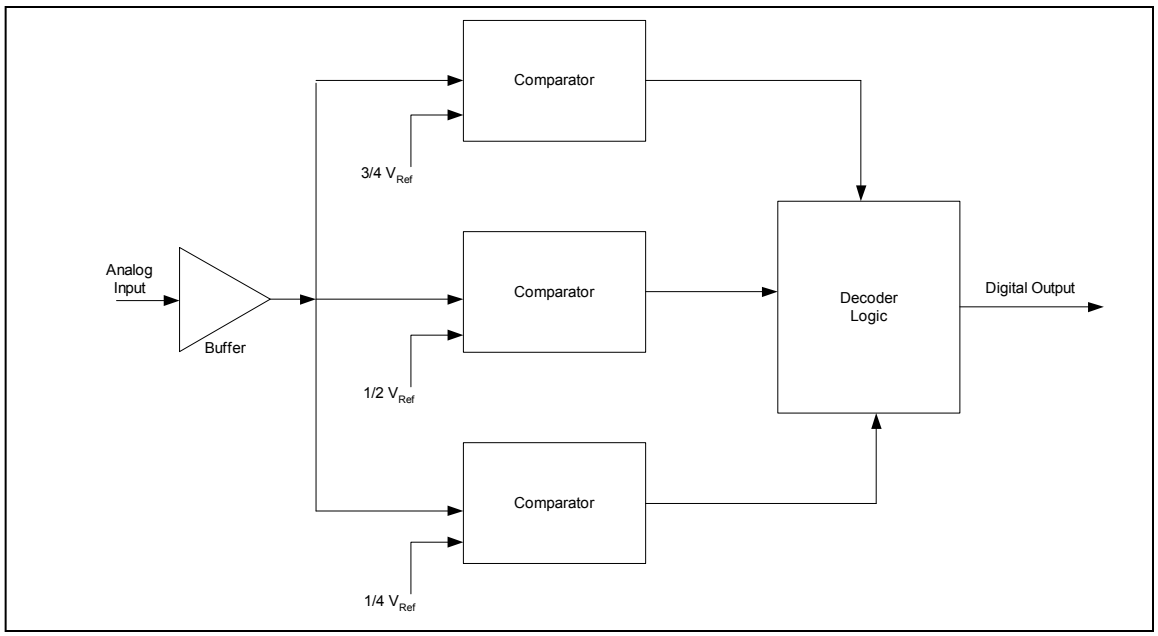

Figure 3. Electronic flash ADC circuit.

An understanding of the operation of Binoptics' devices and electronic flash architectures, therefore, motivates the investigation of a photonic flash ADC version architecture incorporating diamond ring lasers. Figure 4 illustrates such a flash design with ring lasers. Note that Figure 4 only depicts the quantization block, so in effect the RF waveform has been optically sampled using a separate mode-locked laser and an electro-optic modulator to create a modulated optical

pulse train. It should be noted also that in the example, each ring laser output is incident on a detector when operating in a CW direction, and also each laser is biased at 2^n-1 voltage levels which corresponds to 2^n -1 laser powers, where n is the number of bits. The incoming modulated pulses are split 2^n -1 times and each split pulse is injected into a preset biased ring laser.

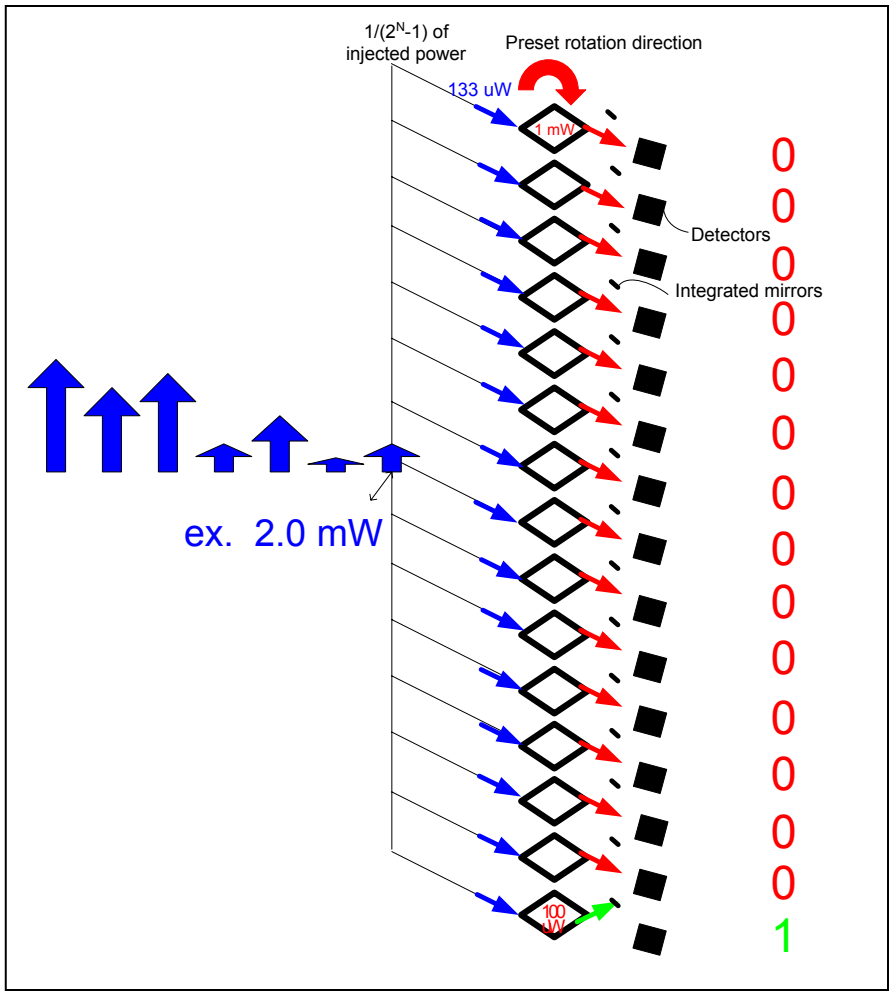

Figure 4. Flash architecture using diamond ring lasers with integrated external mirrors.

For example, if a 2 mW pulse is split equally 15 times, corresponding to a 4 bit architecture, then 133 μW would be incident on each ring laser. Each laser is biased so that there are equal intervals of output power, so for instance, if the minimum channel was at 100 μW and each channel increased with incremental power steps so that the maximum channel was powered at 1 mW, then each interval would be separated by ~ 66.67 μW. When the 133 μW pulse is injected into each laser, a threshold effect occurs if this exceeds the power level at which the laser was operating, making the propagation direction change to the CCW direction. The detector that "sees" the CW light then turns off, indicating a binary "1". This is illustrated by the bottom channel in Figure 4. After this pulse passes, the ring laser reverts back to the original CW direction and waits for the next pulse to arrive.

A preliminary analysis was performed to examine some of the constraints of this system. The assumptions made included a sampling frequency of 10 GHz with FWHM pulse width of 12 ps, a wavelength of 1550 nm, and a minimum bias set for first ring laser to provide 10 μW of output optical power with 5 μW increasing increments for each consecutive ring laser. The injected input power must be greater than the ring laser's operating power in order to switch the laser propagation direction, and a laser output of 10 μW is still well above the dark current of commercial detectors. Table 1 shows power levels needed for various bits in the flash architecture described.

Table 1. Power requirements needed for a ring laser based flash architecture.

# of Bits n	# of Channels $N=(2^n-1)$	Injected Laser Power Required to Switch the Most Significant Channel (mW) $P_m=(N-1)*5\mu W+10\mu W$	Avg. Input Power to Splitter Needed (mW)
4	15	0.080	0.148
6	63	0.320	2.43
8	255	1.280	39.2
10	1023	5.120	629

Assuming 10 μW for the inverter threshold of the least significant channel and a channel-to-channel increment of 5 μW, the input power needed to the splitter is 39.2 mW for 8 bits and 629 mW for 10 bits. For 10 bits and greater, amplification becomes necessary.

InPlane Photonics Inc. manufactures integrated waveguide amplifiers that may be suitable in flash architectures requiring more than 8 bits. A 1x128 integrated waveguide splitter has already been commercially demonstrated by NTT Inc., and a 1x255 and 1x1023 integrated waveguide splitter is within the range of scalable projections by InPlane.

Achieving a 10 GHz photonic ADC appears realistic with most of the key components in a photonic architecture. Commercial high repetition rate, low noise lasers currently operate at 10 GHz and commercial E-O modulators provide 40 GHz operation. Commercial detectors have advanced to 60 GHz rates, which leaves the quantizer to be the limiting component. The question to investigate was, therefore, "Can the ring lasers switch rotational direction and be stable at 10 GHz speeds?" Results described later show that this, in fact, holds true.

The benefit of this photonic flash architecture is that it *significantly* exceeds the speed at which electronic flash architectures currently operate. The closest commercial high speed ADC (by Atmel Grenoble), offered a 2 Gb/s sampling speed with 10 bits of resolution at the time of writing this document. With this suggested photonic approach, there are no electronics needed to

implement a ladder, or thermometer, code of comparators. Comparators will be needed to compare the voltage arriving from the detector, but in this case they will all be set at the same reference voltage. The ring lasers essentially perform the differential comparison of amplitude levels, thereby, significantly reducing the complexity of the electronics needed.

3.2 Successive Approximation

The discussion now focuses on a slower, but higher resolution converter, namely, the successive approximation architecture. These are used primarily where an input signal is continuously varying at high speed or where a succession of inputs is multiplexed at high speed into the A/D converter. This converter requires n steps for encoding to an n-bit binary value, and therefore, requires only half the number of channels of a parallel flash architecture.

The input voltage is fed to one input of the comparator, while the output of the internal D/A converter goes to the other input. Each bit line in the D/A converter corresponds to a bit position in the output register. Figure 5 depicts this architecture. The most significant bit (MSB) output is equivalent to ½ the converter's full-scale voltage range. The conversion consists of starting with the most significant bit and successively trying a "1" in each bit of a D/A decoder. If the input signal is larger than the MSB, a logic "1" is inserted in the MSB position in the output register. If the input is less than the MSB, then a logic "0" is inserted. The circuit then tries the next bit in the circuit. Again if the analog input is larger, a "1" remains for that bit. The procedure continues through to the least significant bit (LSB). At the end of the process, after the LSB has been tried, the binary number in the decoder is the digital equivalent of the analog voltage. The digital output can be taken serially or in parallel fashion.

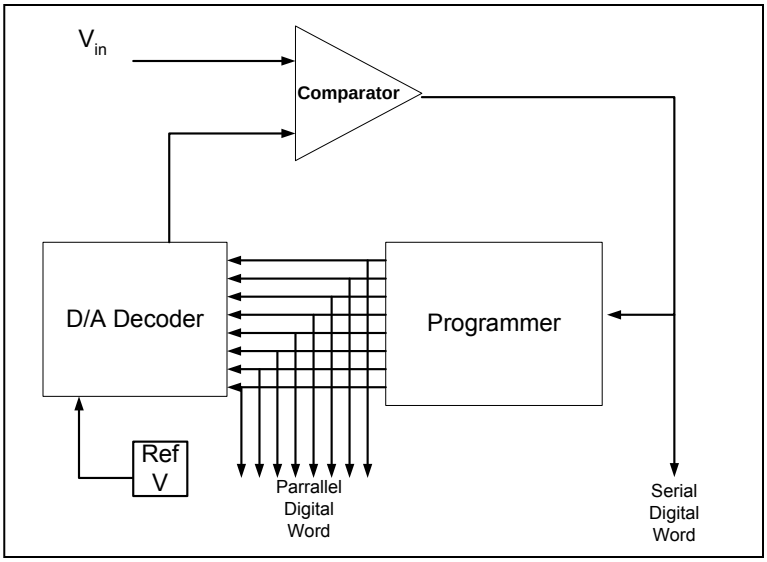

Figure 5. Successive Approximation Architecture.

For example for 6 bits, Figure 6 demonstrates how a digitally generated voltage converges on the analog input level, assuming a full scale voltage level of 10 V and an incoming analog voltage of 3 V.

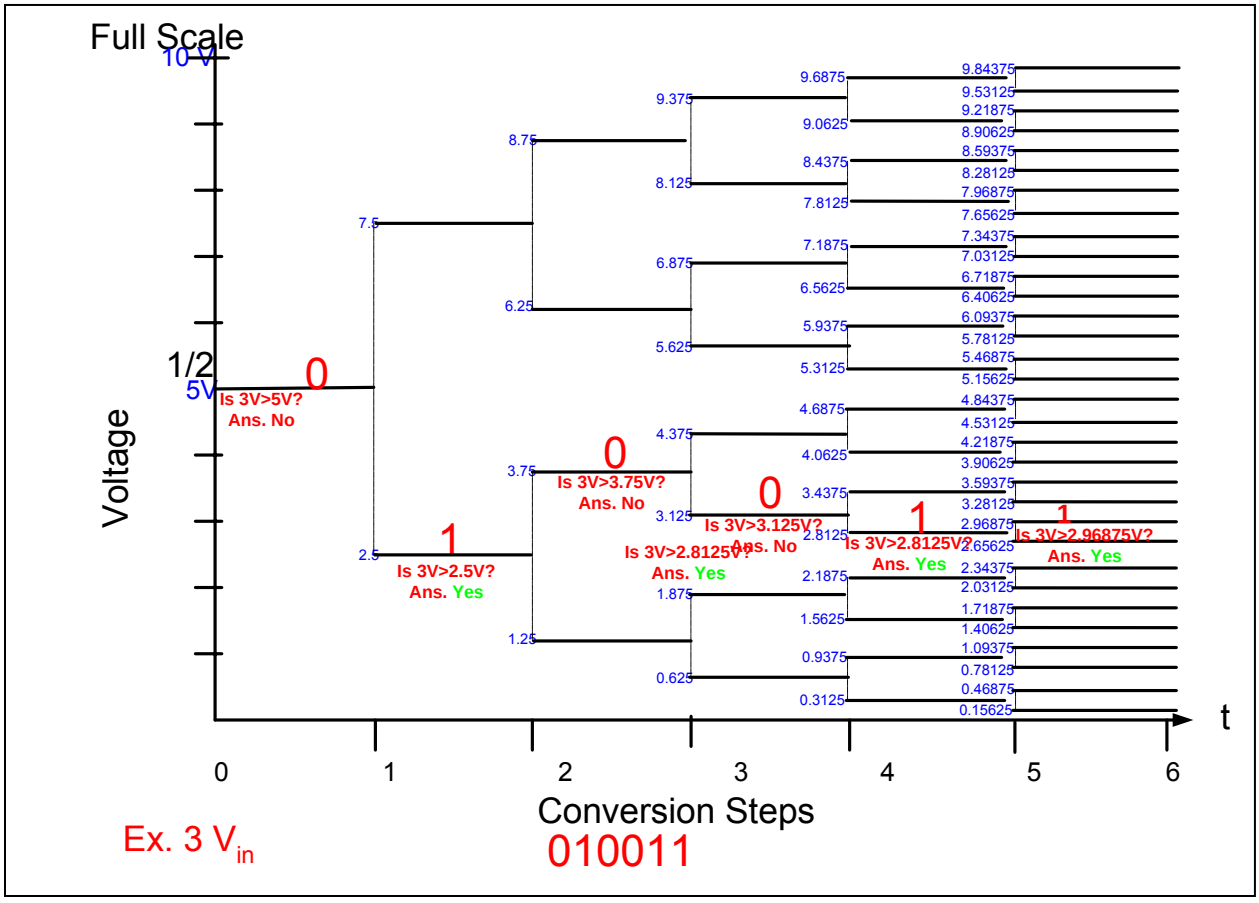

Figure 6. Operation of a 6-bit successive approximation A/D converter for a full scale voltage of 10 V and an incoming analog voltage of 3 V.

The conversion speed of a successive–approximation converter is based on the settling time of the MSB logic ladder network and comparator. This type of converter requires a total conversion time equal to the clock rate multiplied by the number of bits being converted. For a clock rate of 10 GHz, a 12-bit converter would take 1.2 ns; each stage operates at the clock rate.

What photonics potentially offers are clock rates of >10 GHz and photonic logic gates that offer faster "settling times". Using the Binoptics' diamond ring lasers in a successive approximation configuration, it seems feasible to achieve a 12-14 bit converter without the need for amplification at a clock rate of 10 GHz. Figure 7 illustrates the photonic system, again assuming the RF signal has already been sampled optically.

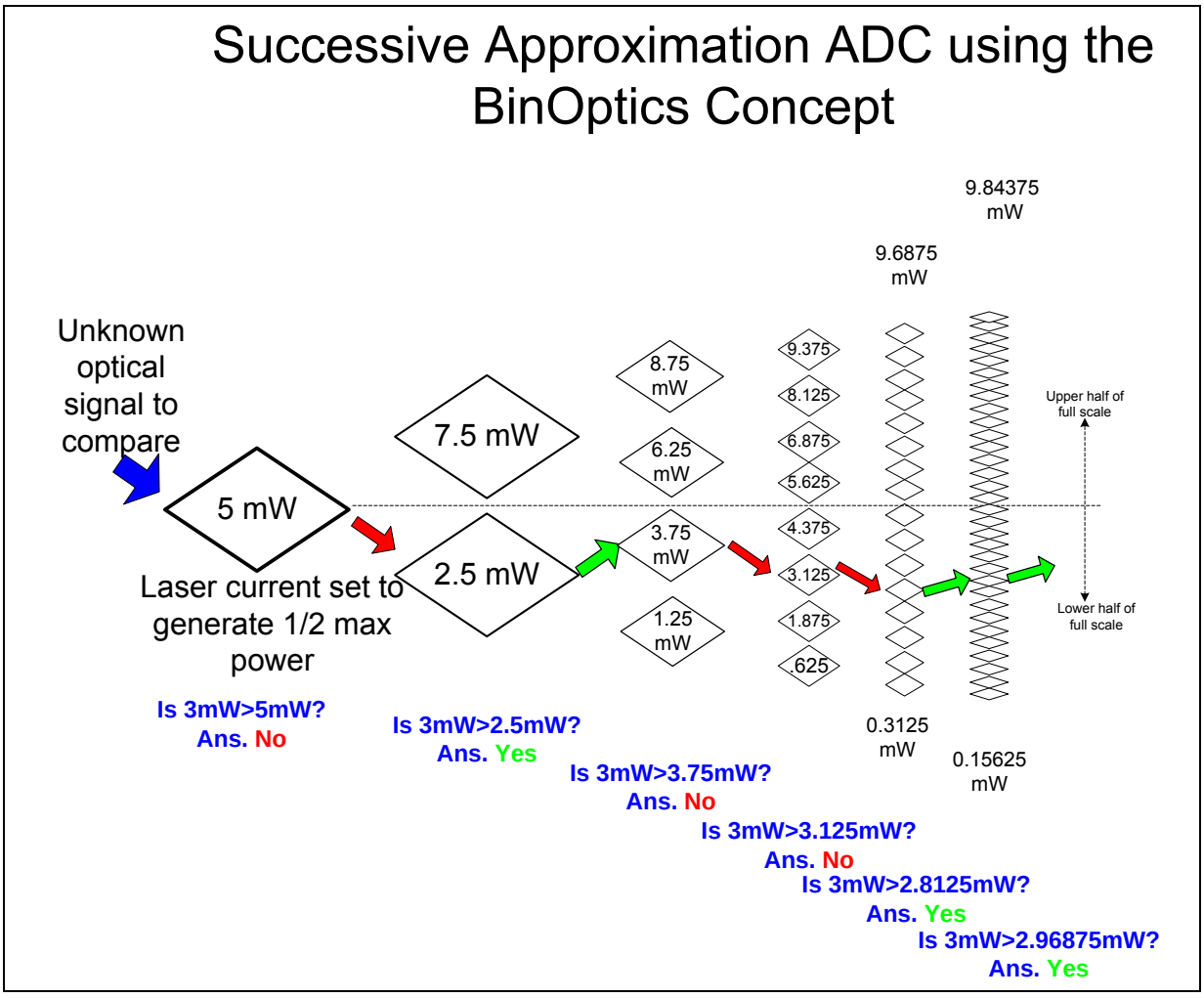

Figure 7. Photonic successive approximation using Binoptics' ring lasers.

In the example system depicted, each ring laser is preset to operate in a clockwise rotation and is assumed to have a maximum output power of 10 mW, in order to correspond to the voltages given in Figure 6. The laser current for the MSB is set at ½ its maximum output power level. If a pulse that enters the first ring laser, depicted by the blue arrow, exceeds the operating power of the ring laser, the laser will switch directions indicating a binary "1", and the light will inject into the upper half of the full scale. If, as in this case, an optical pulse enters the first ring laser with less power (3 mW) than that of the ring laser, the rotational state remains the same and a binary "0" is given for the MSB. The light is injected into the lower ½ of the full scale and is compared against its ½ power level, 2.5 mW. Because these are integrated structures, it can be assumed that there are minimal losses upon exit and entry of successive devices. So the 3 mW input compared with 2.5 mW, gives a binary "1", and the light progresses through the system yielding a digital output representation of the input analog signal.

During initial discussions with Binoptics, it was stated that their ring lasers could operate at up to multiple-tens of milliwatts. Assuming those limitations on the ring laser power, a first level analysis was performed. Table 2 shows the results of the number of channels needed and power separation between each channel for 8-14 bits. Scenarios using a 10 mW full scale output power and a 60 mW full scale output power are also included.

Table 2. Achievable bits using 10 mW and 60 mW full scale operating power. Also indicated are the adjacent power differentials for each case.

# of Bits	8	8	10	10	12	12	14	14
Input Power (mW)	10	60	10	60	10	60	10	60
# of Channels Required	128	128	512	512	2048	2048	8192	8192
Most Significant Channel Power Separation (μW)	156	938	39	234	9.8	59	2.4	15

At first glance, it seems that a major obstacle is in the LSB, since 14-bits require 8192 channels. Binoptics has so far demonstrated 1 x 8 laser arrays structures and sees no fundamental obstacles that preclude fabrication of much larger arrays, if high speed ADCs warranted such development. Isolation between laser channels also becomes a key issue. Binoptics precise fabrication technology has demonstrated isolation between elements on the order of MΩ, which is several orders of magnitude better than other vendors of similar integrated structures. More analysis needs to be performed with regards to system noise, but it is envisioned that a successive approximation approach could successfully provide 12-14 bits of resolution at sampling speeds as high as 10 Gs/s.

4.0 Experimental Results

4.1 Ring Laser Die Testing

Binoptics delivered seven ring lasers in chip format to AFRL/SNDP for investigation. Unfortunately, these devices were not mounted on cooling chips, which contributed to their performance initially not meeting the full potential suggested by Binoptics' investigations[4]. A top-view photograph of the die having four complete devices is shown in Figure 8.

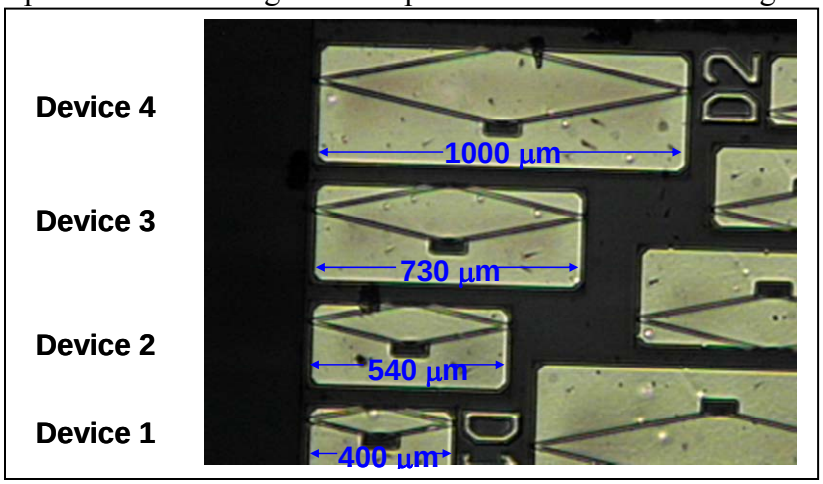

Figure 8. Photograph of devices (A1) received from Binoptics.

Results reported by Binoptics[4] were on individually addressable devices, whereas the lasers delivered were only addressable on one edge, shown by the left edge in the photograph. Figure 9 shows a schematic of the laboratory setup. The lasers were addressed on the left side with lensed fibers, one to inject light and one to collect light for diagnostic purposes, such as monitoring the emitted wavelength with an optical spectrum analyzer (OSA). A Keithly source, Model 228A, delivered the drive current to power the ring laser throughout most of the experiments discussed here. Light was injected in path A, unless otherwise noted, using a New Focus tunable laser, model 6300 Velocity. Light exited the biased cavity bidirectionally and was scattered off the devices sitting on the right side. Free space optics collected the scattered light and focused it onto two detectors (the type depended on the bandwidth needed at the time), and the signal was observed with a Tektronix oscilloscope (channel 2 green and channel 3 orange). The blue trace indicated the trigger signal sent by an HP 3312A function generator, which was in phase with the optical light being injected imposed upon using a JDSU Mach-Zehnder (MZ) modulator. The output was amplified using an erbium-doped fiber amplifier (EDFA) and sent through an Eigenlight, an in-line fiber power meter. This power meter had a dialable attenuator allowing the injected light power to be controlled and varied from +4.2 dBm to -20 dBm, corresponding to 2.1 mW to 10 μW, respectively.

Testing involved ring bias current vs. output power, gain quenching vs. bias current, gain quenching vs. injected light power level, and low frequency encoded injection examinations ranging from 200 Hz-7 MHz. Injected light power levels ranged from 3 μW to 1.5 mW.

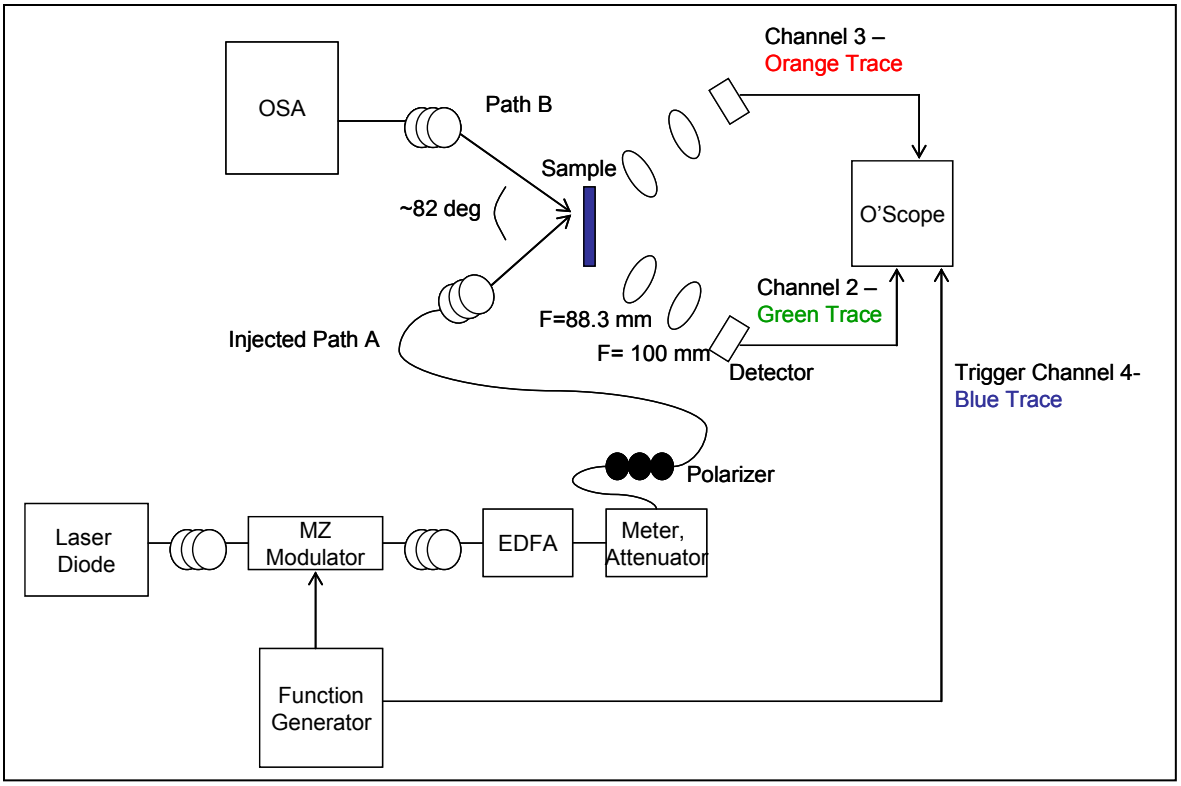

Figure 9. Experimental setup.

Figure 10 maps the current vs. power plots for the operating ring lasers. The current level for one of the exiting beams in Device 2, L=540 um, turned over at approximately 110 mA. This is suspected to be due to the lack of chip cooling so that heating of the cavity started to quench lasing in that direction.

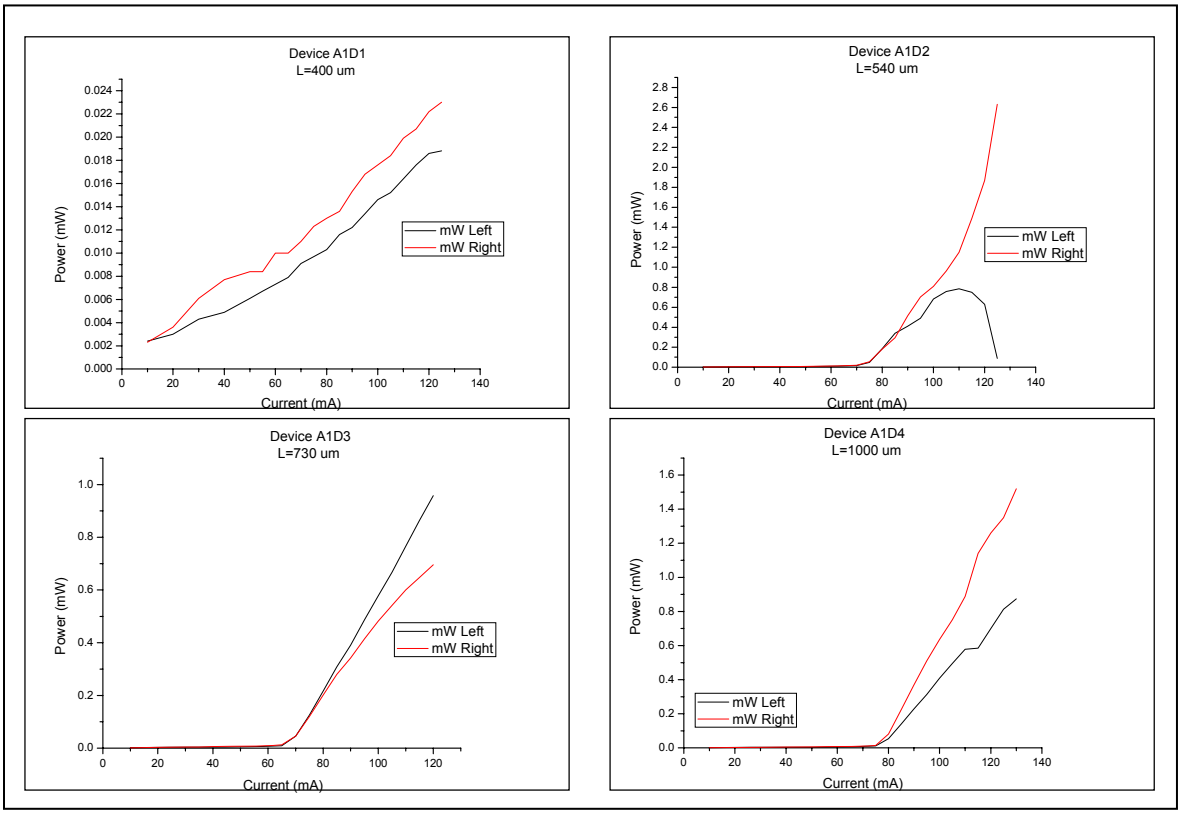

Figure 10. Output power performance of chip A1 devices.

4.1.1 Injection Wavelength Investigation

These are Fabry-Perot type devices and generate multiple wavelengths. If the cavity is not perfect, the main resonance peak may have some competition. Figure 11 shows output spectrum with two strong competing modes at λ~1.53575 μm and λ~1.5368 μm for Device 2 on chip A1 (A1D2) with L=540 μm.

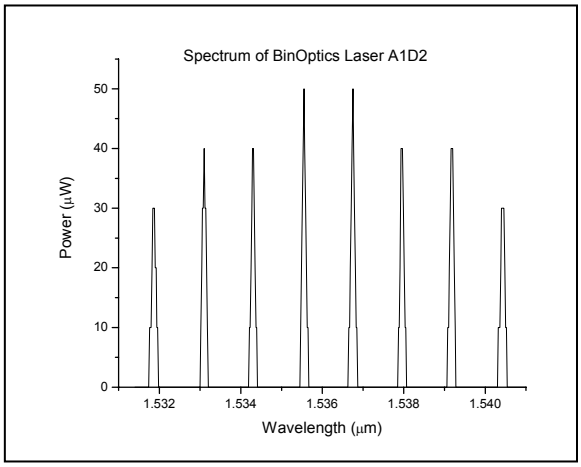

Figure 11. Resonant wavelengths of the A1D2 ring laser.

When light is injected into the ring laser cavity and aligned with one of the ring cavity modes, the ring laser side modes can become suppressed by 35 dB. Alignment does not have to be with the peak mode of the ring laser to force suppression. These traits are clearly shown in Figure 12 (from devices later supplied from Binoptics).

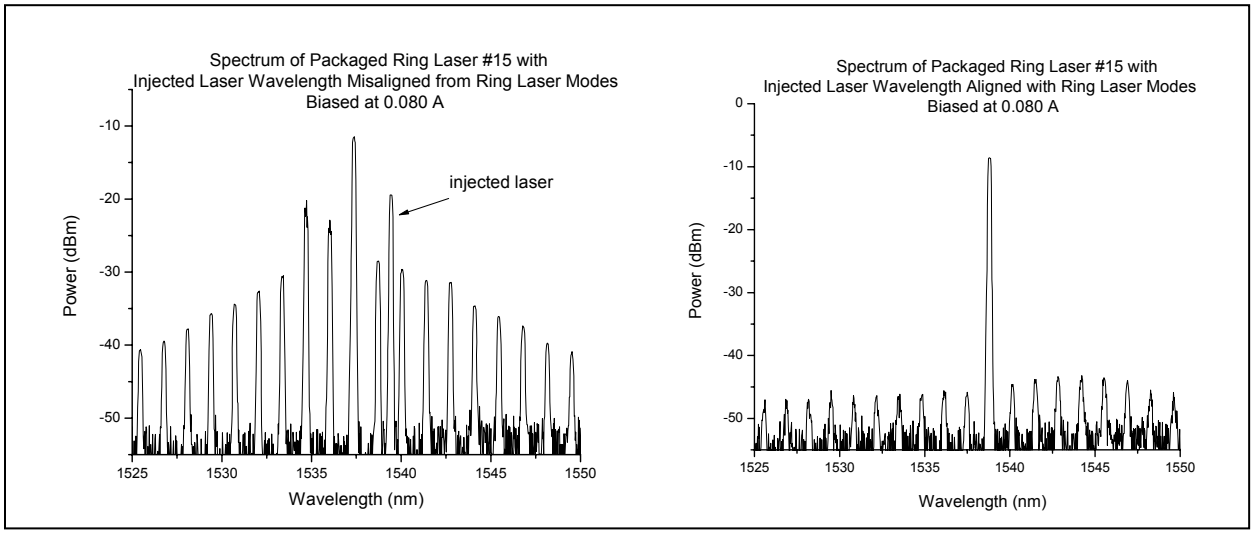

Figure 12. Optical spectrum when laser injection wavelength is a) not aligned with ring laser modes, and b) aligned with a mode.

For device A1D3 Figure 13 shows switching at 200 Hz with 80 μW of light injected to the maximum peak resonance, while Figure 14 shows 200 Hz switching with 80 μW injected into a

side mode resonance. The optical spectrum was captured before and after each optical injection. When the injected light was aligned to a resonance peak, the spectrum's shift in wavelength is suspected to be due to cavity heating. The magnitude of the switching was less when aligned to a side mode peak.

Fiber alignment and facet back reflections also affected switching response. The ripple on the channel 3 trace changed as the fiber position changed. Ideal operation would involve anti-reflection coating the surfaces that are in line with the laser cavity.

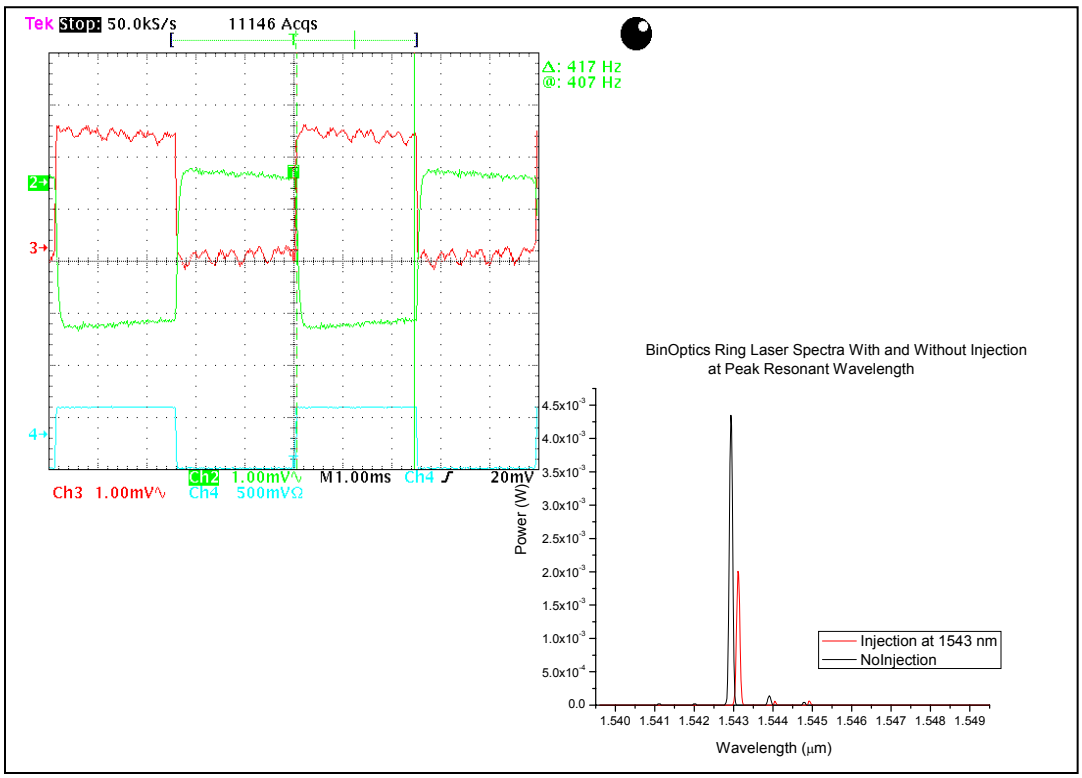

Figure 13. Switching A1D3 device at 200 Hz with 80 μW of injected power.

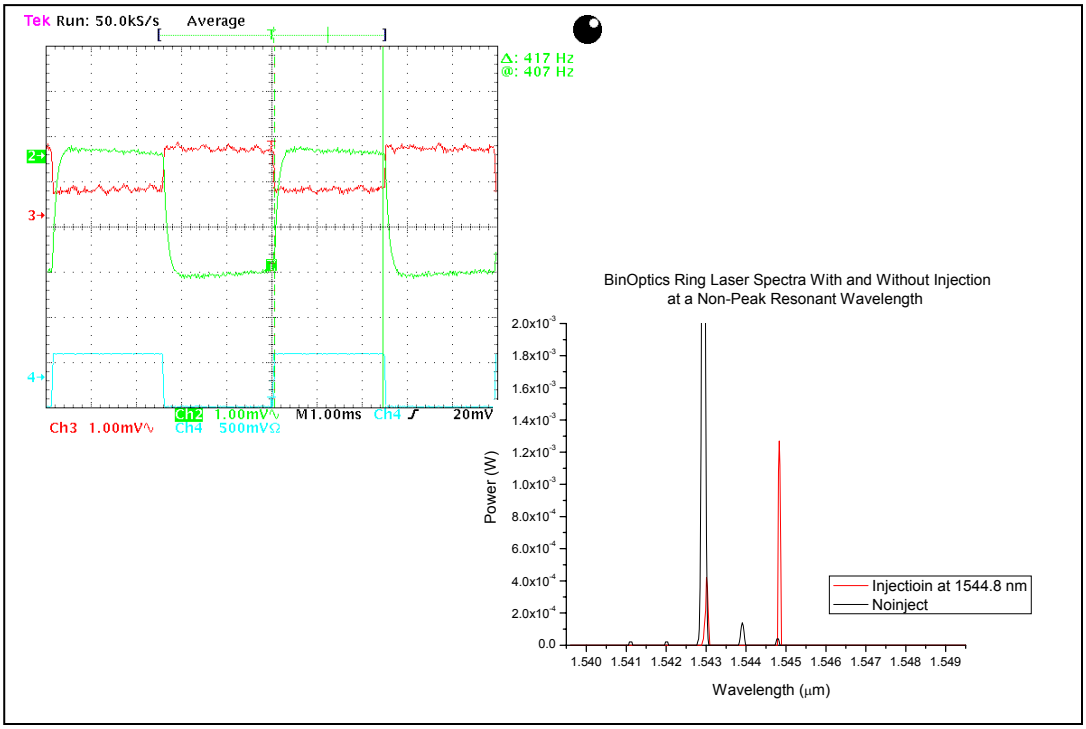

Figure 14. A1D3 switching is shown but reduced in magnitude when the injected wavelength is matched to a smaller resonance peak, 1544.8 nm.

Figure 15 “time stamps” heating effects and illustrates changes in switching magnitude and optical spectrum for A1D3. The magnitude of the switching decreased over a period of 8 minutes when injecting at peak resonance. The optical spectrum shows a competing mode emerged from what was initially a smaller resonance, and after 8 minutes the resonances completely shifted.

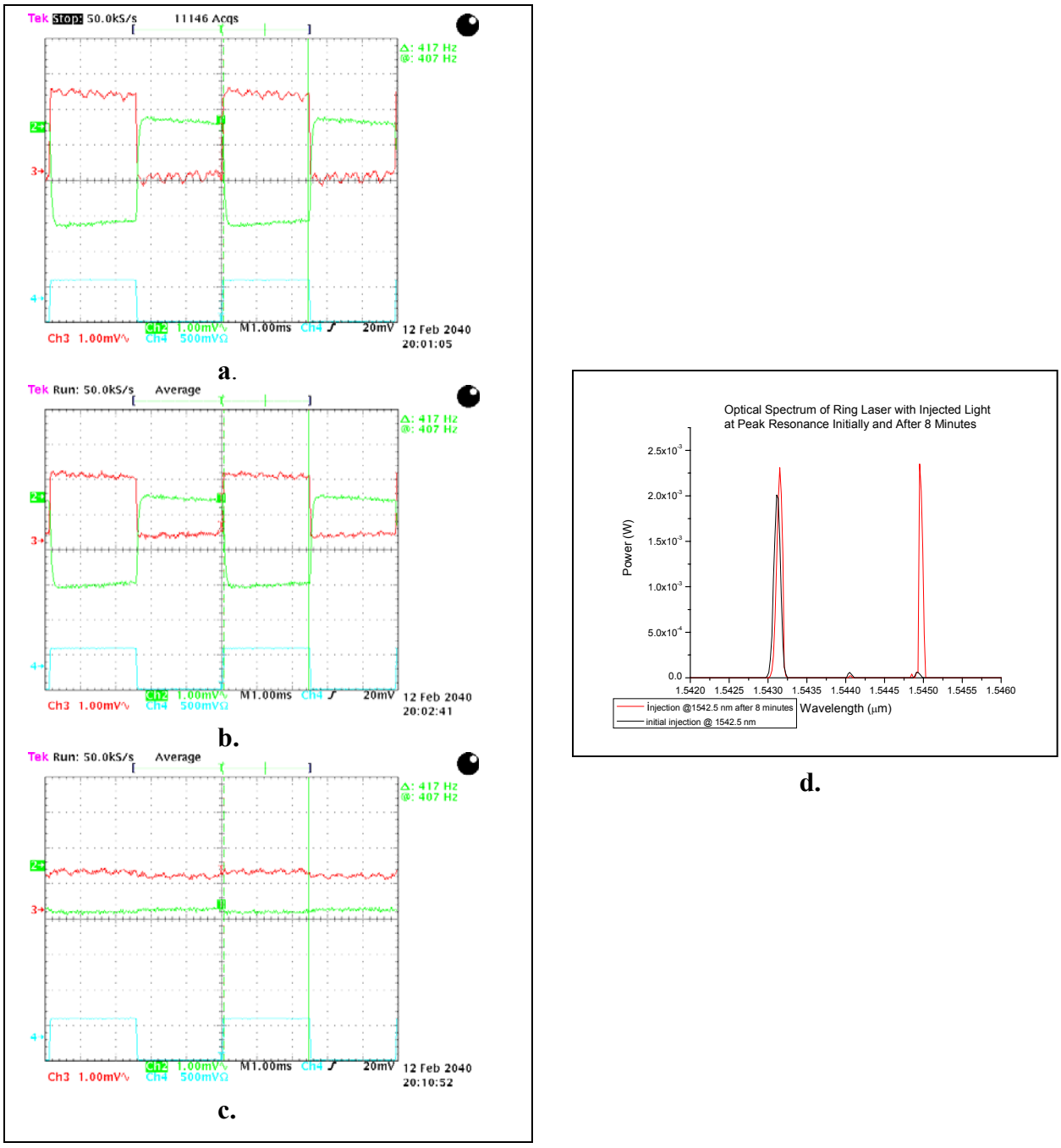

Figure 15. A1D3 switching a) initially with injection at main resonance; b) magnitude decreased after 1.5 minutes; c) magnitude almost disappeared after 8 minutes. d) Optical spectrum shown for initial switch and after 8 minutes.

4.1.2 Injection Frequency Investigation

Binoptics demonstrated switching in the gigahertz regime with approximately 100 μW. However, in SNDP's uncooled chip setup, switching past 3 KHz was severely degraded at 80 μW injection levels and not visible on the oscilloscope minimum scale of 1 mV/division. In an attempt to surpass the limited frequency observation, higher injected power was used even though it would induce more heating. Power injected into A1D3 was amplified and filtered to provide an output 1.5 mW.

Switching with this higher power when injecting at the main resonance peak was not possible indicated by the traces remaining in phase shown in Figure 16 for 700 Hz, 3 KZ, 700 KHz modulation frequencies. The ring laser had a favored propagation direction signified by the unbalanced current vs. power curves in Figure 3, and it remained propagating in the favored direction when injected at this higher power level. However, aligning with a much smaller side mode resonance peak, switching was readily observed as shown in Figure 17. It is, therefore, suggested that with 1.5 mW injected at the main resonance peak, heating dominated and quenched any switching. It was not fully clear what was actually occurring until further gain quenching experiments were performed.

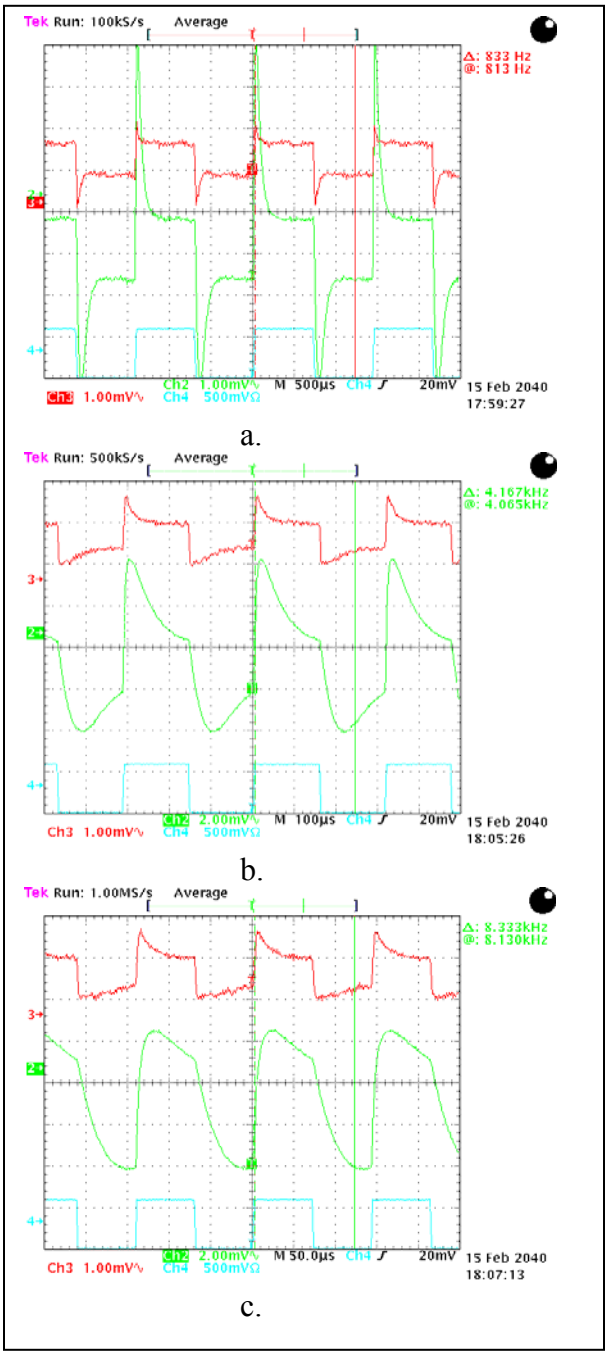

Figure 16. Light is in-phase in each channel when injecting 1.5 mW at the peak resonance wavelength. a) 700 Hz modulation; b) 3 KHz modulation, c) 7 KHz modulation.

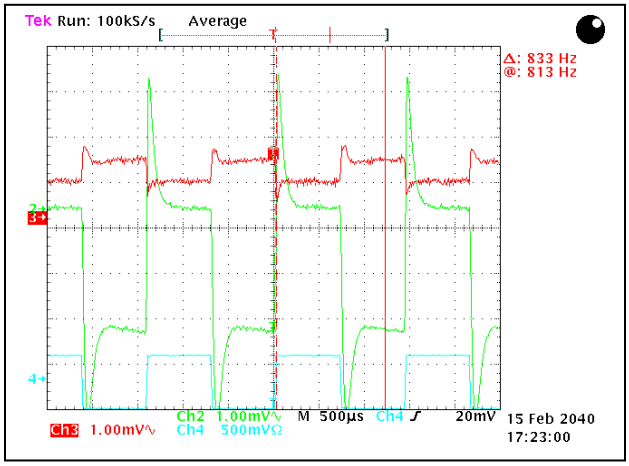

Figure 17. Switching at 700 Hz at 1.5 mW when injected wavelength is aligned with a smaller side resonance peak, λ=1544.2 nm.

A more curious observation was that very strong switching was observed when the injection arm was switched to path B at 1.5 mW. Figure 18 shows effects at 700 Hz, 7 KHz, 70 KHz, 700 KHz and 7 MHz using the different injection arm. With successive increases in frequency, the switching magnitudes decreased, and lack of switching occurred at 7 MHz. Injected power was increased to 10 mW, but MHz operation was still not possible.

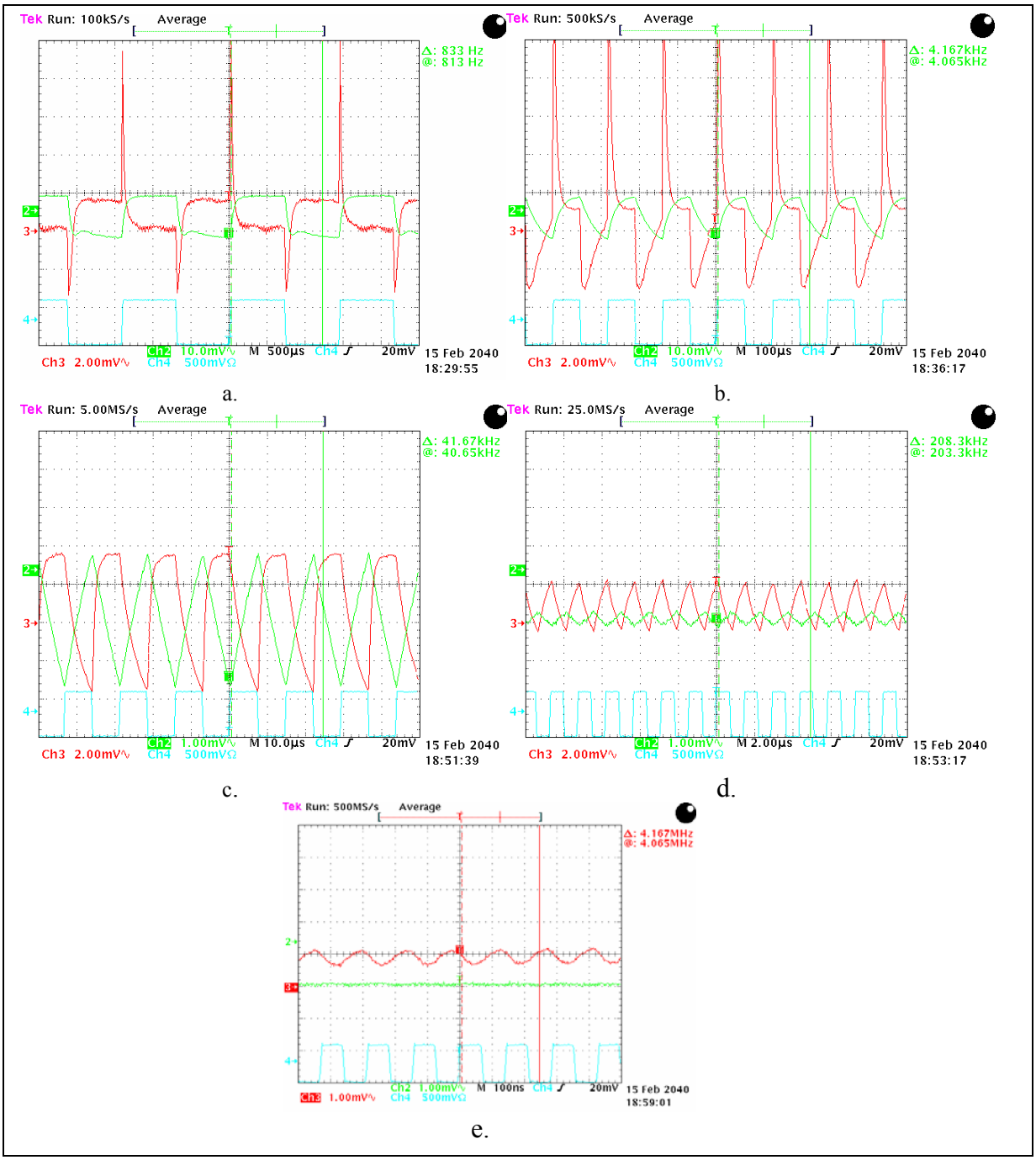

Figure 18. Switching observed when injecting in to path B @ 1.5 mW at main resonance, λ=1542.9 nm at a) 700 Hz; b) 7 KHz; c) 70 KHz; d) 700 KHz; e) 7 MHz.

4.1.3 Gain Quenching Investigations

Gain quenching can be observed when the directionality of the counter-propagating mode changes as a function of bias current or injected light power level.

Using the same experimental setup, device A1D2 was examined with a rate of 700 Hz. Injection path B was used, and as before channel 2 on the oscilloscope trace was green and channel 3 on was orange, while the blue trace indicated the trigger and was in phase with the optical light being injected.

Figure 19 gives a base line switching pattern when the bias current on the ring laser was set to 0.0850 A, well above threshold, and the injected power level was approximately 80 μW, similar to the initial power level used in the prior laser experiment.

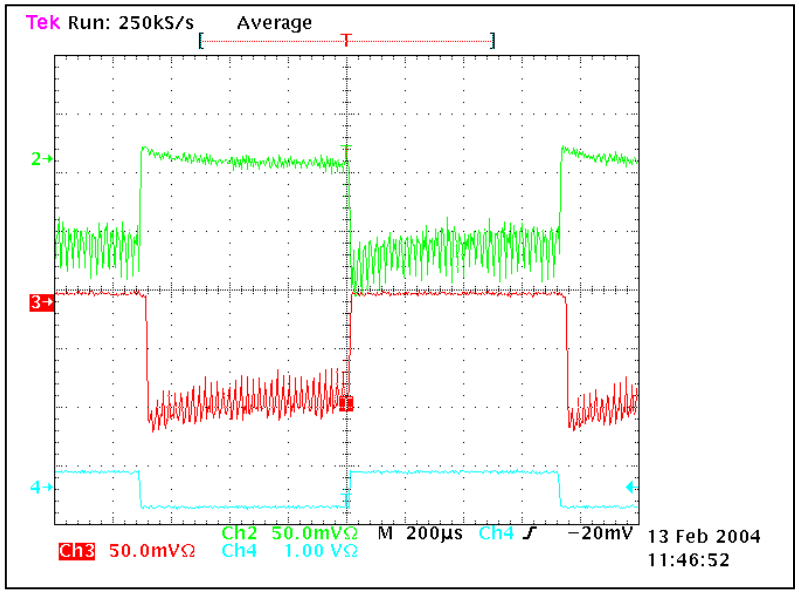

Figure 19. Baseline switching for device A1D2 with bias current set to 0.0850 mA and the injected power level 80 μW.

Bias current was examined first, and after each level reduction an adjustment of the injected wavelength was needed to ensure the injected light remained resonant with the ring cavity light. The bias current was reduced to 0.078 A, just above threshold, without noticing a change in directionality.

The effect of varying the injected light power level was checked next. Laser A1D2 was biased at 0.079 A, high enough above laser threshold, and the injected light power levels sequentially reduced from ~80 μW to ~3 μW. Figure 20 demonstrates that the phase of switching did not change for this power range meaning these levels did not affect gain quenching. At the 80 μW the rise edge in the counter propagating mode starts to demonstrate a peaking effect, which was very strong in the larger cavity device A1D3 at higher injected powers.

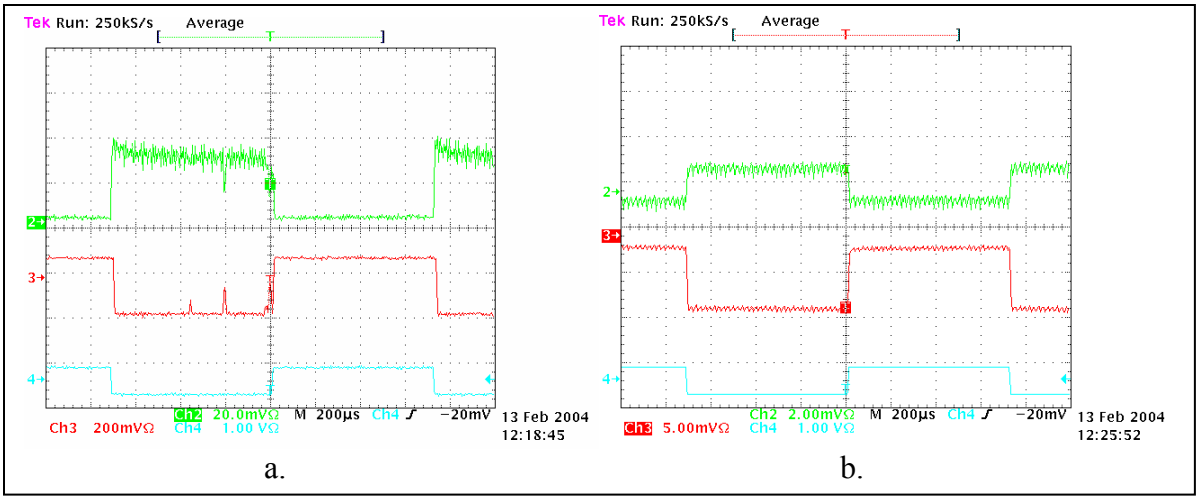

Figure 20. a) Ring bias at 0.079 A, injected power ~80 µW; b) Ring bias at 0.079 A, injected power ~3 µW.

Gain quenching was not observed for this ring laser using low bias current levels and low injected light levels. This was good news suggesting that the co- and counter-propagating modes would not compete to hinder switching activity at these levels. Unfortunately, it was still not clear what the effect would be using higher injected levels, since some heating or quenching behavior was indicated in Figure 16 with the A1D3.

In an ADC architecture the LSB is of significant concern because if it cannot be resolved precisely, errors occur. In the analysis using ring lasers in a successive approximation architecture, the values associated with the LSB were in estimated to be in the range of 100's of microwatts. The capacity to reduce by two orders of magnitude the threshold power, 3 µW shown here, allows for many more channels and, hence, a much greater number of bits.

4.1.4 Possible Q-Switching Behavior

Q-switching allows the production of light pulses with extremely high peak intensity. Initially the laser medium is pumped while the Q-switch device prevents feedback of light into the gain medium, thereby, producing an optical resonator with a low Q-factor. This produces a population inversion, but laser operation cannot yet occur since there is no feedback from the resonator. Since the rate of stimulated emission is dependent on the amount of light entering the medium, the amount of energy stored in the gain medium will increase as the medium is pumped. Due to losses from spontaneous emission and other processes, after a certain time the stored energy will reach some maximum level at which the medium is said to be gain saturated. At this point, the Q-switch device is changed from low to high Q, allowing feedback and the process of optical amplification by stimulated emission to begin. Because of the large amount of energy already stored in the gain medium, the intensity of light in the laser resonator builds up very quickly; this also causes the energy stored in the medium to be depleted almost as quickly. The net result is a short pulse of light output from the laser, known as a giant pulse, which may have a very high peak intensity.

The Q-switch itself may be a mechanical device (e.g. a shutter, chopper wheel or spinning mirror placed inside the cavity), some form of modulator such as an acousto-optic or electro-optic device, or a passive saturable absorber material. In the case of the diamond shaped ring laser, one of the gain paths may act as a mechanism.

Figures 16-18 all depict a large spike artifact on the waveforms and occurred when the injected power level was relatively high, 1.5 mW, for the A1D3 device. It was suspected that the behavior was related to Q- switching and was dependent on cavity size. The A1D3 device cavity was larger than A1D2, and spiking did not occur at 80 μW injection. On the contrary, Figure 21 shows small spike formation for the A1D2 device with 80 μW injection biased at 0.079 A. When injecting into path A, it seemed that for the co-propagating wave, when the population inversion became too high, indicated by peak on green trace, a loss was observed in the counter-propagating red trace for all cases.

To examine the effect further, the bias current on A1D2 was increased while keeping injected light power constant. However, mapping Q-switch or spike formation in this manner was futile because heating rendered unstable switching very quickly at different bias levels. Switching became unstable because the resonance continually shifted, making tuning of the injection wavelength problematic. Thus, it became apparent that cooling was necessary to drive the laser beyond 0.080 A.

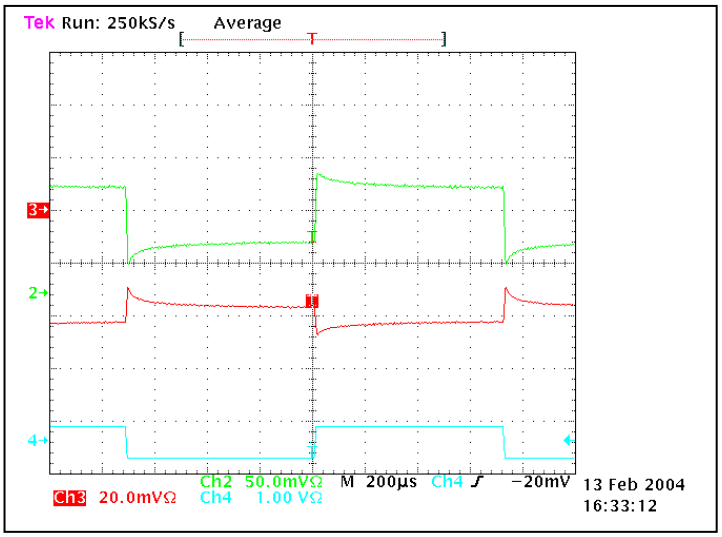

Figure 21. Small spiking effects occurred when biased at 0.079 A and injected with 80 μW, which follow the rise/fall edges on channel 2 (green trace) and channel 3 (red trace).

Varying light power while keeping constant bias current on A1D2 was an alternative way to map Q-switch or spike formation. The injected power levels ranged from -19 dBm to 4 dBm corresponding to 11 μW to 2 mW, respectively, and the bias level was kept constant at 0.079 A. Figure 22 maps the interesting sequential results. Each trace has large voltage levels suggesting that Q-switching may in fact be occurring.

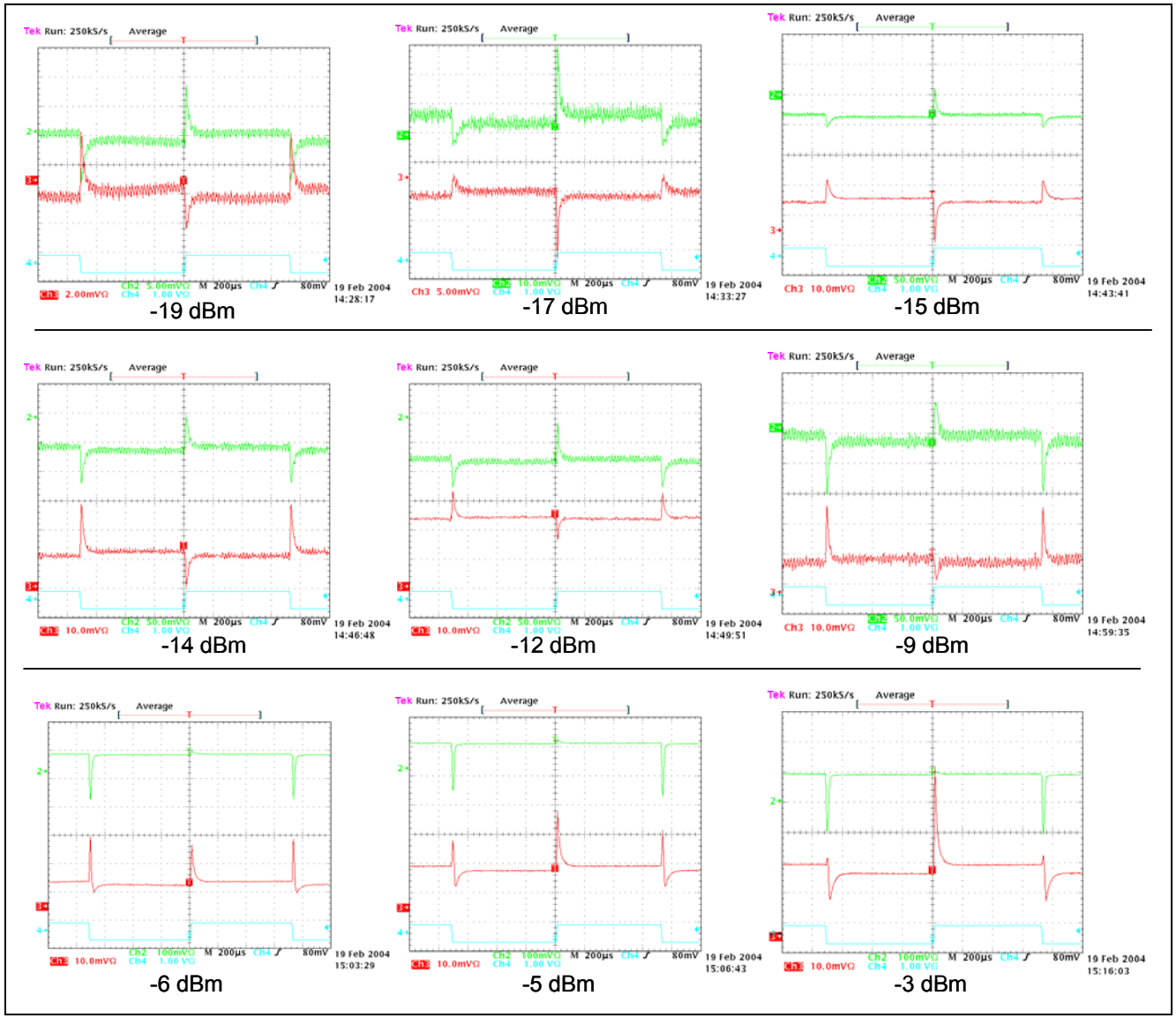
Tek Run: 250kS/s Average
-19 dBm
Tek Run: 250kS/s Average
-17 dBm
Tek Run: 250kS/s Average
-15 dBm
Tek Run: 250kS/s Average
-14 dBm
Tek Run: 250kS/s Average
-12 dBm
Tek Run: 250kS/s Average
-9 dBm
Tek Run: 250kS/s Average
-6 dBm
Tek Run: 250kS/s Average
-5 dBm
Tek Run: 250kS/s Average
-3 dBm

a.

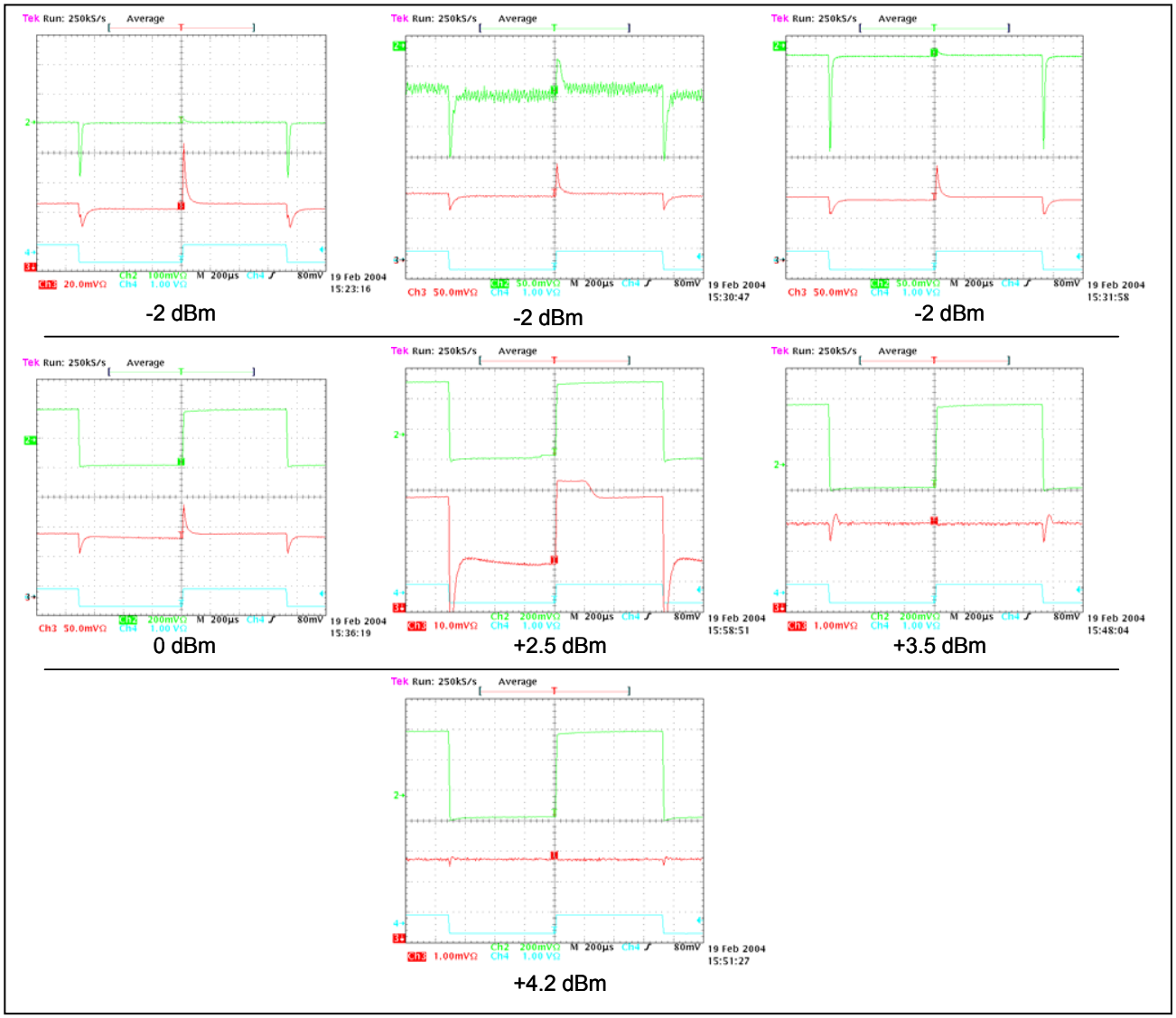

b.

Figure 22. Results of injecting various powers into ring laser.

The thumbnail plots of Figure 22 encompass many experimental observations. At -19 dBm switching was observed but the DC levels drifted and the waveforms seemed noisy. At -17 dBm the DC drift quieted down but the waveforms were still noisy. It was unclear if the activity caused triggering problems or if it was truly noise. Switching with -15 dBm became much quieter. At -14 dBm the peak on channel 3, corresponding to the rising edge of the light in the "on" state, started to decrease, while the valleys corresponding to the falling edge of the trigger start to increase. At -12 dBm and -9 dBm, channel 3 amplitudes changed and at -9 dBm the traces seemed noisy, indicating that the laser was changing its modal state.

At -6 dBm for channel 3, the trace that was following the rise edge of the trigger became inverted and in phase with the trigger, while for channel 2 the trace that followed the rise edge of the trigger significantly decreased and remained in phase. The peaks that follow the fall edge of the trigger remain in a switched phase for both channels. However, channel 3 overshot on the fall edge of the trigger while channel 2 doesn't. At -5 dBm, the effect was the same, but stronger, and at -3 dBm, stronger yet. It seemed that the injected light levels were approaching a point of overdriving the laser, or gain quenching, because at -2 dBm, the traces became in phase with each other.

At 0 dBm an extreme change occurred. Channel 2 became a square wave trace following the trigger without a peaking effect, while channel 3 still had the peaking effect. Taking note of the voltage scale, channel 2 was on 200 mV/div; the highest scale used to date, while channel 3 was relatively strong, 50 mV/div, it decreased quickly as the injected power increased.

At 2.5 dBm channel 2 remained uniformly square while channel 3 approached a square wave function, but remained with a Q-switching effect associated with the edges. The trailing edge and rise edge clearly involved different mechanisms.

At 3.5 dBm, channel 2 became stronger, and channel 3 diminished in amplitude but had an oscillation associated with the fall edge. At 4.2 dBm almost all the power resided in channel 2 perhaps indicating full gain quenching.

4.1.5 Laser Die Experimental Summary

Switching up to 700 KHz with an injection power of 1.5 mW was observed; this became dependent on the injection path at higher power levels. Switching was observed with a minimum of 3.2 μW. Behavior similar to Q-switching was observed with injection at various power levels for two distinct laser cavities. Back reflections played an important role and had a significant effect on switched behavior. Heating effects were definitely witnessed, affecting gain quenching and possibly carrier dynamics. Better device layout and experimental setup including laser cooling are needed to better understand the switching mechanics.

Relaxation oscillations at different ring laser bias levels were not observed at the low frequencies. This was encouraging and suggested that the carrier dynamics would not interfere with the mechanism of switching needed for optical flip-flopping applications.

These lasers demonstrated significant promise in that they switched cleanly when biased properly and injected with proper power levels. Efforts were put forth to package a set of lasers in a stable platform that would facilitate more extensive investigations.

4.2 Packaged Ring Lasers

As stated, it became quite clear that die devices posed several difficulties for applications testing: reflections from the access port facets interfered with the injection process; the free-space coupling efficiency was far from optimal; and heating and temperature related effects were not stabilized. The key issues were largely overcome when Infotonics Technology Center partnered with Binoptics Corporation to provide three integrated/packaged versions to AFRL for detailed characterization. Technical advances were required to implement the waveguide's geometry so as to access all active ports with optical fiber. Metal ferruled lensed fibers with anti-reflection (AR) coatings were incorporated into existing thermo-electric (TE) cooled packages. The multi-port packaging and optimization procedures were reported by Stoffel, et al., in the 2006 Electronic Component Technology Conference submission[5].

Frequency and injection power limits were investigated with these packaged devices. Another objective was to determine if the induced "switching" of mode intensity was primarily due to the stimulating effect of injection, rather than a variation of carrier density, particularly since the former could enable much higher laser response rates.

It is well known for semiconductor lasers that increasing drive current or using a shorter cavity increases the relaxation oscillation frequency. Also an increase in the number of quantum wells in the structure increases the gain which is proportional to the square of the relaxation frequency. Such effects have been thoroughly examined at Binoptics in single cavity Fabry-Perot designs, with relaxation frequencies in excess of 15 GHz being achieved and still higher ones being attainable. The effects of all-optical methods for the modulation, as pursued here, provide an alternative approach. Injected light levels of 2 μW induced switching in prior die testing experiments, but here levels were varied from 100 μW to much higher ones that approached the intensity of the free-running laser, so that relaxation effects could be observed in different parameter regimes.

The operating characteristics and phenomenology results are presented the remainder of this paper. A description of the packaged devices and the experimental layout in section 4.2.1 is followed by the experimental results for square pulses in section 4.2.2 and single frequency inputs in 4.2.3. Some injection wavelength detuning effects are discussed in 4.2.4, and followed by the theoretical model in chapter 5.

4.2.1 Experimental Setup

In Figure 23 a representative diamond shaped ring laser is shown left, while a prototype packaged ring laser is shown right. The ridge waveguides had width of 3.5 μm with a mode-field size of approximately 3.3 μm that permitted fairly efficient single mode fiber coupling, and the

laser output was polarized horizontal to the substrate. Saturation current (I_{sat}) was ~ 160 mA, while threshold current was ~ 57 mA for the particular module tested. Table 3 describes characteristic parameters, output power (P_{out}) at I_{sat} and return loss (RL), measured for the packaged module.

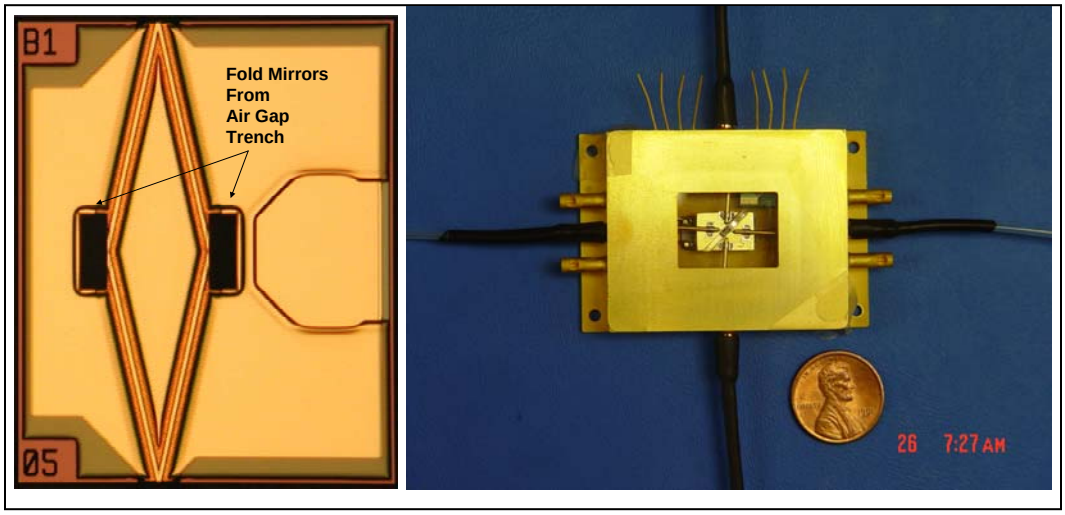

Figure 23. A representative diamond shaped ring laser shown left with a prototype packaged ring laser shown right assembled by Infotonics Technology Inc.

Table 3. Characteristics of Packaged Ring Laser (Module #13)

Fiber Channel	**A1**	**A2**	**B1**	**B2**
P_{out} at I_{sat}=160 mA	1.49 mW	2.09 mW	2.06 mW	1.70 mW
RL	-23.23 dB	-29.31 dB	-27.8 dB	-27.8 dB

Figure 24 illustrates the experimental setup, similar to Figure 9, used to characterize the packaged devices. A Keithly source delivered the drive current of 80 mA to power the ring laser throughout most of the experiments discussed here. A New Focus tunable laser, model 6300 Velocity, provided an injected power of approximately 500 μW. An erbium-doped fiber amplifier (EDFA), Pritel Inc. LNHPFA-30, was used to provide higher power levels to the JDSU Mach-Zehnder (MZ) modulator, and a polarization controller set the proper state for the modulator. An Agilent signal generator, model 83650B, delivered the RF sinusoidal signal to the modulator, and a Krohn-Hite Corp. precision DC source, model 523, controlled the modulator bias, which was set to operate on the negative slope of the transfer curve. The output from the modulator was connected to an in-line polarization maintaining (PM) fiber power meter, Eigenlite PM 422, which had a dialable attenuator to vary injected light power with a range of +10 dBm to -20 dBm (10 mW to 10 μW), and Discovery Semiconductor 30S Lab Buddy detectors (3 dB @ 18 GHz) monitored the switching waveforms. An Agilent 86142B optical

spectrum analyzer (OSA) captured the ring laser and injection laser spectrum, while an HP 54750A oscilloscope with a 50 GHz module displayed the output waveforms.

The signal generators used to impose the waveforms, or encoding, on the modulator were interchanged between an Anritsu 5 Gb/s, 16 bit pulse pattern generator, model MP 1608A, and an HP 83650B, 20 GHz, sinusoidal frequency generator. The MZ modulator was biased at quadrature in both cases. For the digital patterns, amplification was used to increase the 2 volt signal to near the V_π value of 5 volts, so that a "zero" logic signal corresponded to a modulator minimum output, which was near zero, and a logic level of "one" corresponded to the modulator maximum. Because a broadband amplifier distorted the encoded pulse patterns from the PG in certain parameter ranges, precautions were taken to ensure that the regimes tested were free of distortion.

For the sinusoidal input signals, amplification was not required because input signals less than V_π were sufficient to exhibit the switching effects, and a zero reference level was not essential. The sinusoidal driving signal applied to a MZ modulator yields a sine wave in the small signal regime, or linear region of the MZ transfer curve. When amplifying the applied signal the general form of the transfer curve becomes $\sin(A\sin(\omega t))$ which is a Bessel function of the first kind. In other words, nonlinear characteristics are manifested gradually with increased signal in the form of higher order effects. These small effects can be detected using a spectrum analyzer before they are witnessed by a change of the waveform's shape. Amplification was therefore used only to maximize the signal to a level that did not exhibit noticeable distortion of the waveform's shape.

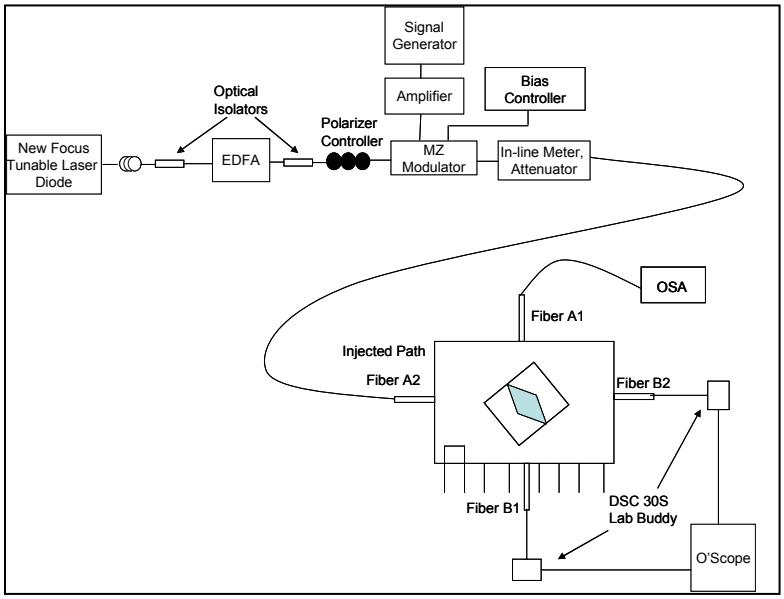

Figure 24. Experimental setup schematic for packaged devices.

Unless otherwise noted the data resulted from injecting into port A2; the clockwise (CW) mode followed the injected path and corresponded to port B1 output, while the counter-clockwise (CCW) mode corresponded to port B2 output, as depicted in Figure 24.

4.2.2 Digital Encoded Injection

The lowest speed investigated with the pattern generator was 100 Mb/s, with a positive logic bit pattern of 1 on 3 off. Figure 25 shows the positive logic pattern sent from the pattern generator to the MZ modulator (left), and unless noted the patterns in this paper were positive and either 1 on 3 off or 1 on 1 off. The right side of Figure 25 shows the device response at 100 Mb/s. Approximately 1 mW average optical power was injected into the ring laser cavity when it was operating at the higher drive current of 120 mA. The extinction ratio exhibited is defined by equation 1 and is effected by injected optical power. The CW mode typically exhibited larger amplitude, and the injected light seemingly experienced some gain.

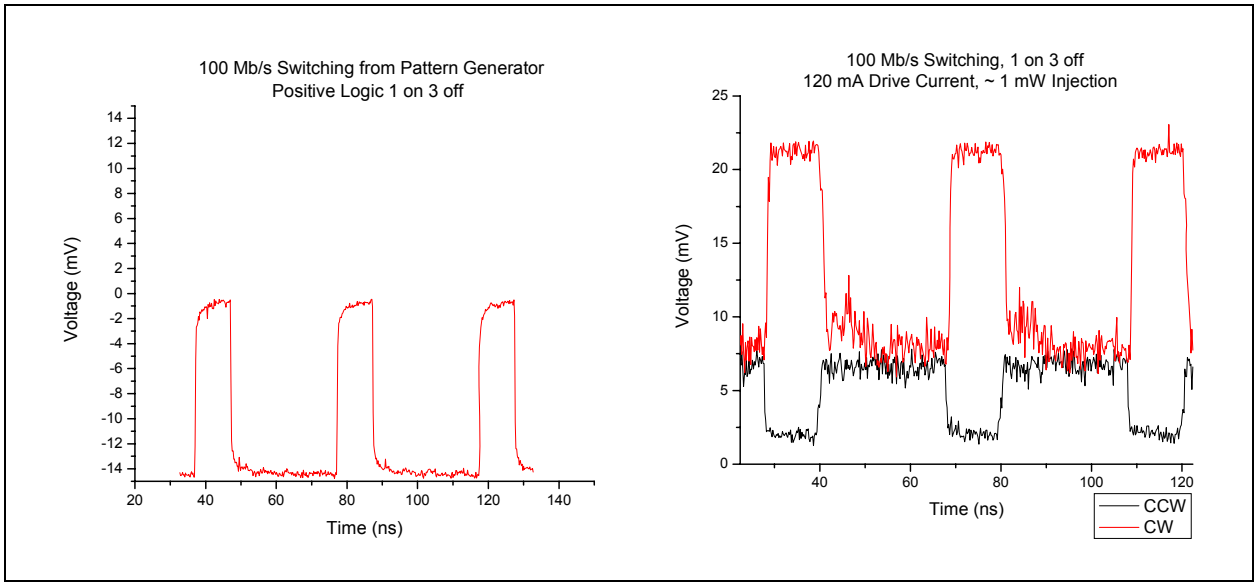

Figure 25. Signal out of the pattern generator imposed on the MZ modulator for 100 Mb/s positive logic pattern 1 on 3 off (left). 100 Mb/s switching, bit pattern 1 on 3 off (right).

Figure 26 shows results for a 1 Gb/s pattern (1 nsec injected pulse width), which implies a 250 MHz repetition (rep) rate for the complete 1 on 3 off pattern. Results for both ~ 100 μW and ~ 800 μW average injected optical powers are shown. For the CCW mode the extinction ratio, defined by,

$$\text{Ext. ratio (dB)} = \log \frac{(V^2_{max})}{(V^2_{max})} = 9 \text{ dB (CCW)}, \quad (1)$$

increased from approximately 4 dB to 9 dB with the higher injected power. More importantly, the counter-propagating mode not only responded, but could be driven down very close to a true zero, ie. no light in the path. The structures observed in the output waveforms may be related to relaxation oscillations corresponding to ~ 0.8 GHz, calculating from the first oscillation peak at ~ 25.2 ns for the 800 μW injection case. Shown in Figure 27 is the difference between 1 Gb/s and 4 Gb/s operation. The stronger oscillations in the 4 Gb/s case may be related to the higher

frequency components of the square wave or the relaxation oscillation limit. In both cases the output pulse formation is broadened.

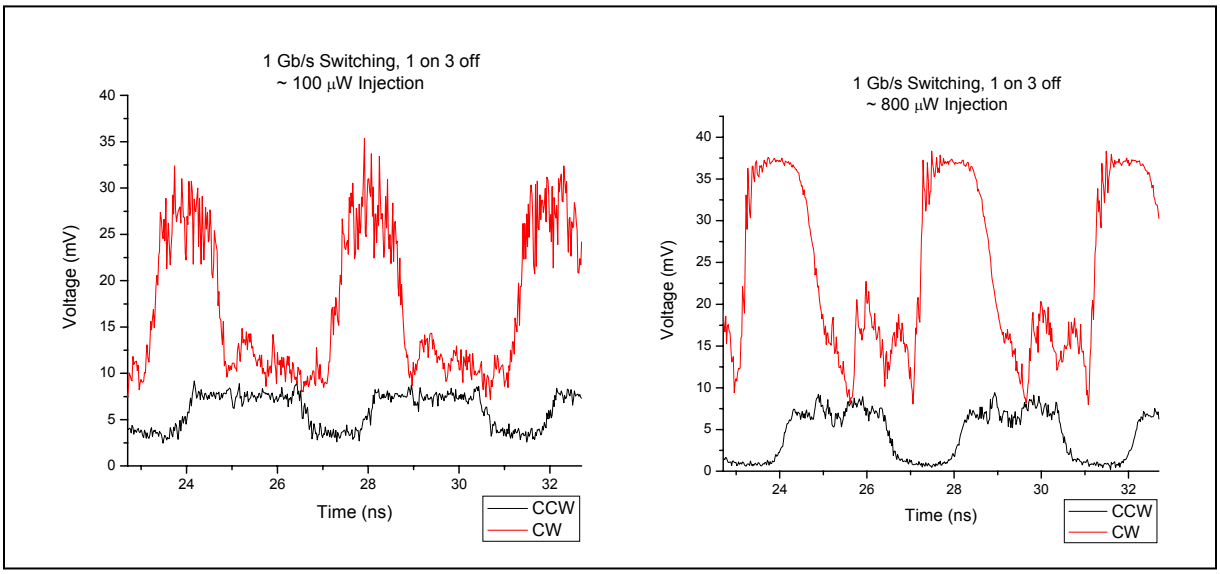

Figure 26. Injection using pattern generator with a 1 Gb/s bit pattern of 1 on 3 off for 100 μW and 800 μW injection.

Injecting the 4 Gb/s (250 ps pulse) positive logic bit pattern, 1 on 3 off, actually corresponds to a 1 GHz pattern rep rate. Figure 7 depicts that the oscillations, ~ 4.5 GHz, in this configuration were more prominent than the 1 GHz sinusoidal case

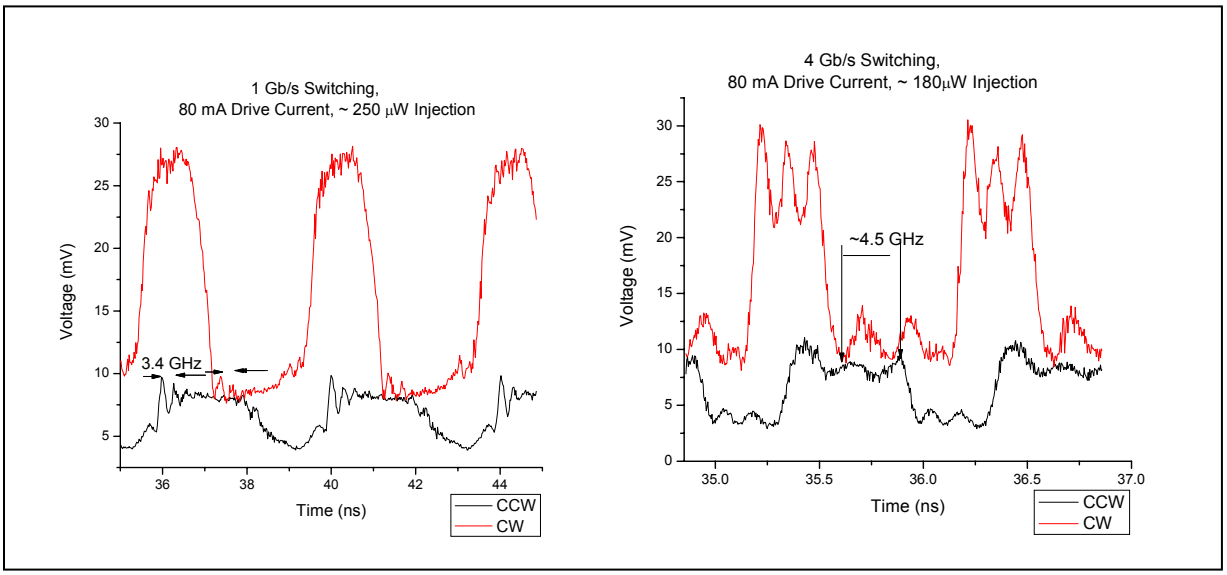

Figure 27. Oscillation patterns change from 1 Gb/s bit pattern of 1 on 3 off to 4 Gb/s bit pattern with the latter being very strong.

Figure 28 illustrates 4 Gb/s negative logic 1 on 3 off, i.e. 1 off 3 on, with a lower optical power injected. This case did not seemingly exhibit pulse broadening, but the pulse envelope was not as square shaped as in the positive case. The reason for this difference cannot be fully explained by

the usual rise and fall time responses because of the interaction between the two counter-propagating modes. Although, it was suspected to be due to RF amplifier limitations.

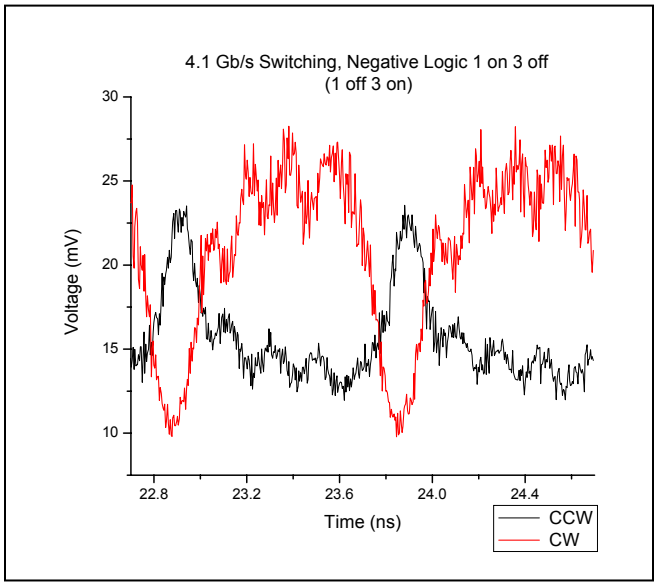

Figure 28. Four GB/s negative logic 1 on 3 off – which is really 1 off 3 on, with ~ 170 µW injected.

Operation of the pattern generator was limited to 5 Gb/s; for a shorter input pulse, the data was considered in Figure 29 measured by Binoptics on an initial unpackaged device[4] with 600 µm round trip cavity length. The figure shows that for a 100 ps (10 Gb/s) pulse the laser still switched, and the co-propagating trace (bottom right) shows the injected pulse to be reproduced with sufficient fidelity to support selected high speed digital operations. Though the magnitude of the oscillation may have been enhanced by reflections internal to this unpackaged device, the ~ 4 GHz value is in the expected range for such a cavity relaxation oscillation. This was directly supported by observing that increased drive current increased the frequency of the observed oscillation.

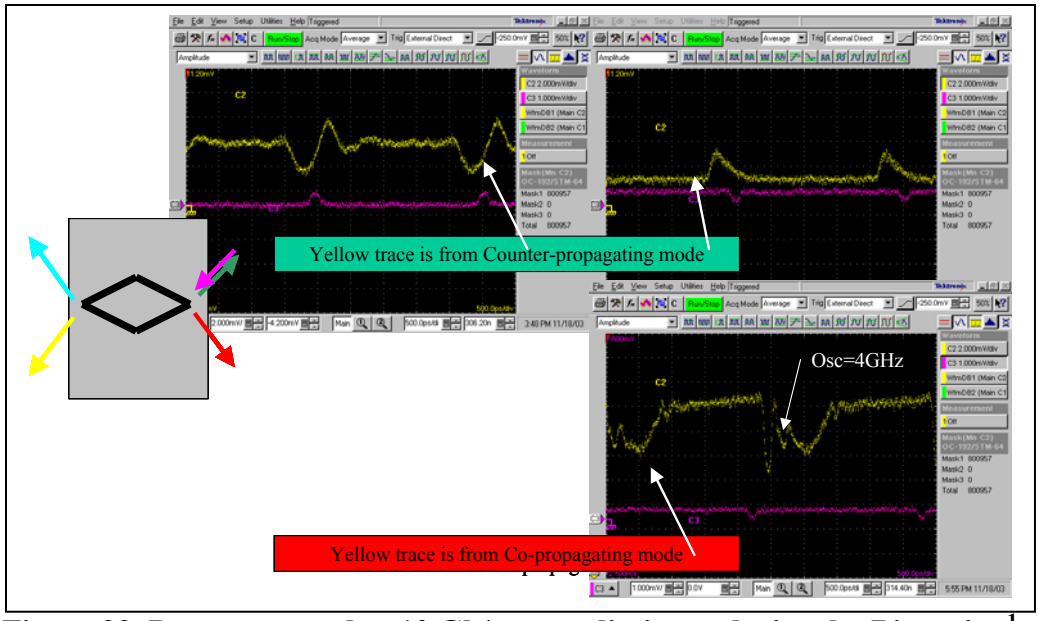

Figure 29. Data measured at 10 Gb/s on preliminary devices by Binoptics.[1]

4.2.3 Single Tone Injection

To observe higher frequency effects, a sinusoidal signal generator was also used for the injected waveforms. No relaxation related oscillation effects were exhibited in those waveforms, but it was observed that higher frequencies required higher injected powers to maintain a given extinction ratio. Figure 30 compares the responses for 8 GHz with 100 μW and 800 μW injected, showing much higher extinction ratio for the latter case. The extinction ratio for the CCW mode increased with increased injection, and for ~ 800 μW injected the extinction ratio for 8 GHz remained over 4 dB. Figure 30 also shows the extinction ratio reducing to < 3 dB at 12 GHz and virtually no response at 15 GHz, respectively, which seems to indicate the bandwidth of the laser because the 3 dB point of the detector was > 20 GHz.

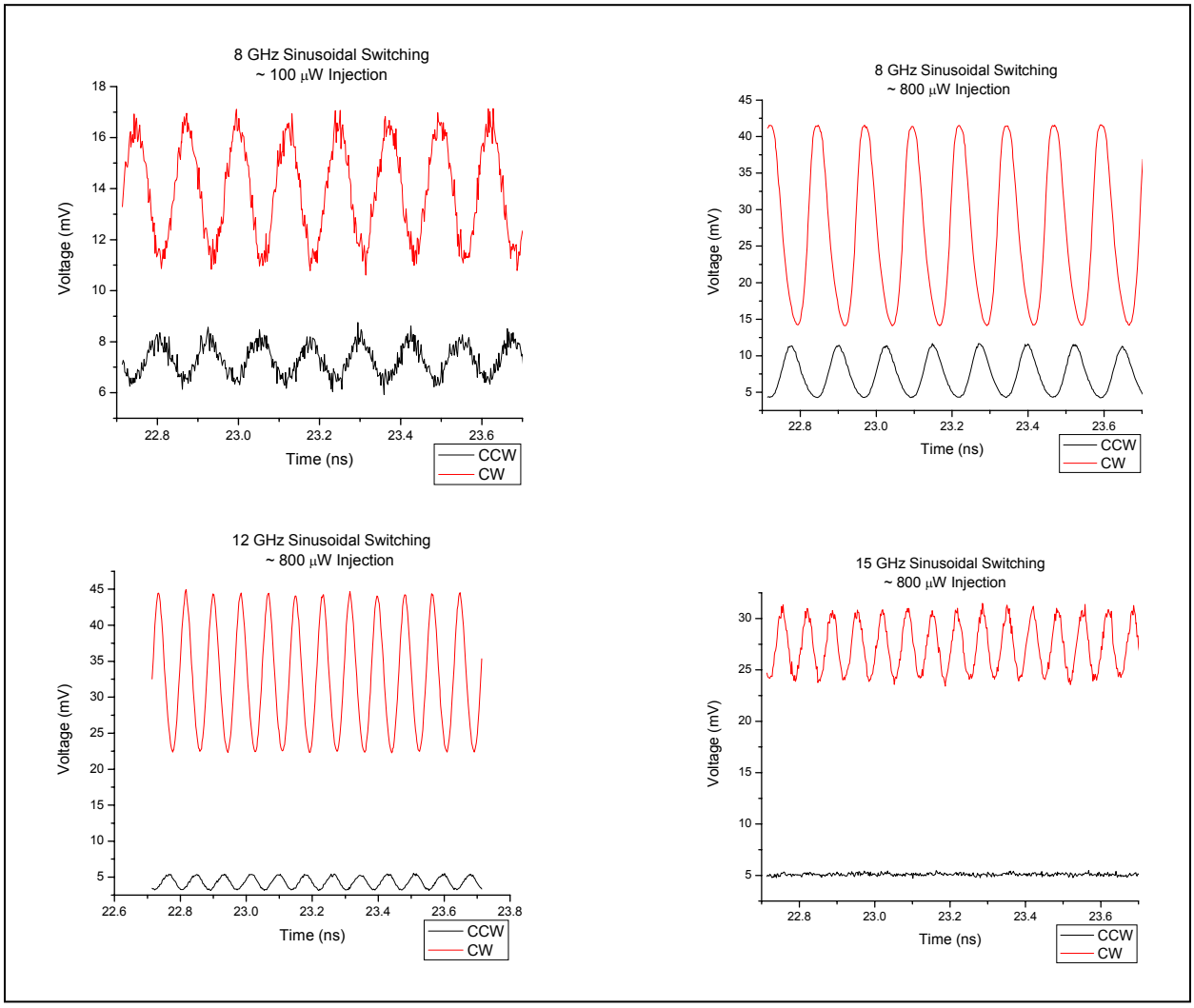

Figure 30. Eight GHz sinusoidal modulation for 100 μW and 800 μW injected powers with the extinction ratio reducing to < 3 dB at 12 GHz and virtually no response at 15 GHz at 800 μW injected powers.

Typically in semiconductor lasers, the relaxation oscillations will increase in frequency with an increase in drive frequency. These diamond shaped lasers exhibit similar behavior when injected with higher power rather than changing the drive current shown in Figure 31. No response is expected when the drive current of a diode laser is directly modulated beyond its relaxation frequency, yet observations, also shown in Figure 31, show an enhanced response. Operation beyond 4-6 GHz occurred for time-varying optical injection. The observed cutoff near 15 GHz in Figure 30 could imply that the relaxation effects still play a limiting role. More research is necessary for a better understanding of the effects.

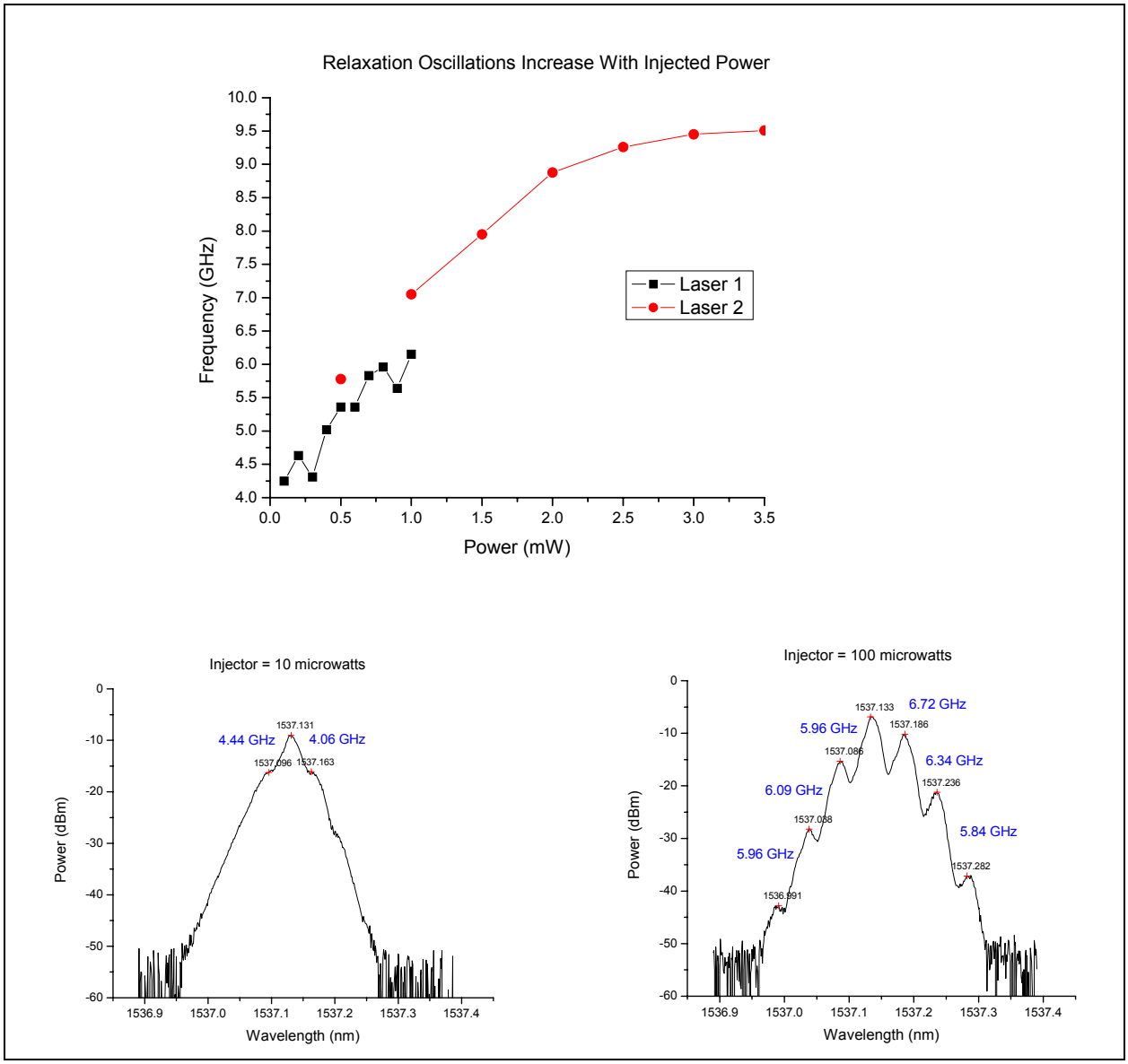

Figure 31. Bandwidth enhancement possibilities for diamond shaped laser cavities using optical injection to increase the oscillation frequencies.

4.2.4 Detuning of Injection Wavelength

The wavelength (de)tuning sensitivity was not obvious at lower driving frequencies (f), but at higher frequencies, such as 10 GHz, the RF modulation sidebands imposed on the wavelength center line were resolvable on an OSA. It was observed that optimal switching occurred when the injected wavelength was detuned from the peak of the ring laser by the magnitude of the driving frequency. The frequency offset for optimal switching was also verified at 4 GHz and 1 GHz., At frequencies below 1 GHz, peaks could not be resolved with available equipment. The

observation for zero detuning the switching response was extinguished is addressed in the theoretical section of chapter 5.

At such high frequencies the injected wavelength could also be detuned by 2f, so the +/- 2nd adjacent sideband became aligned with the center peak of the ring resonance, and with sufficient power, injection locking could occur at those sidebands. The effect was two detectable wavelengths propagated in the same direction, which simulated frequency doubling in the output. Figure 32 shows the switching output when the injection was detuned by 10 GHz along with the optical spectrum of the injected signal and an overlay of the ring resonance.

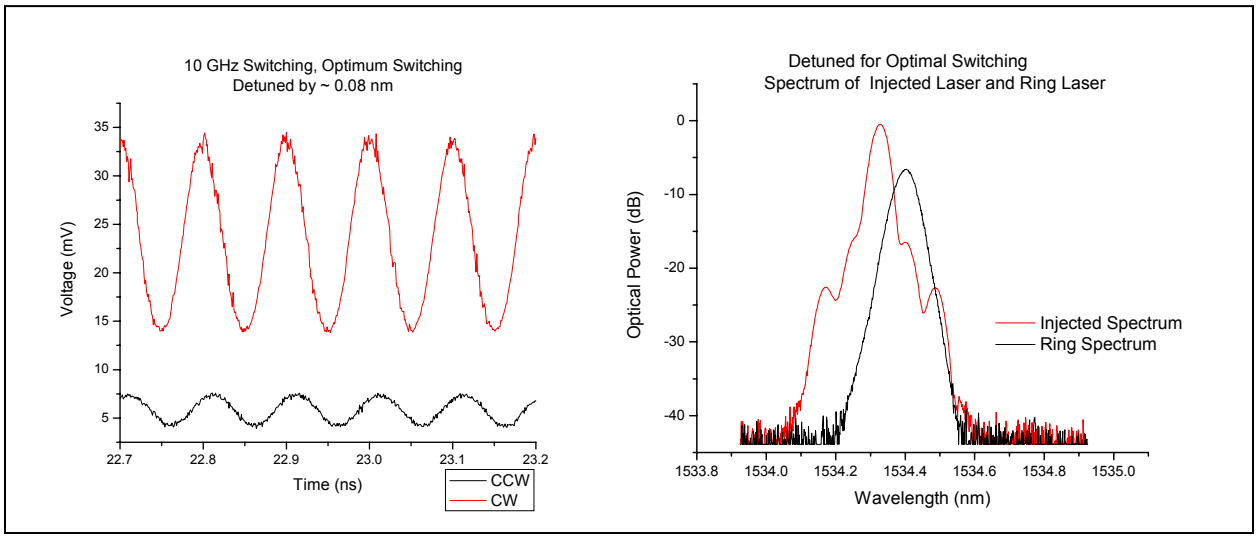

Figure 32. Ten GHz switching with frequency detuned by ~ 10 GHz, and optical spectrum of overlaid injected wavelength and ring laser resonance showing wavelength detuning of ~ 0.08 nm (10 GHz).

Figure 33 illustrates the evolution of the 10 GHz waveform as the wavelength was progressively detuned through the doubling effect. When completely detuned, the waveform disappeared, indicating complete misalignment and suggesting that the power level available (optical or RF) in the 3rd sideband was not sufficient for inducing the resonant enhancement to drive the switching mechanism.

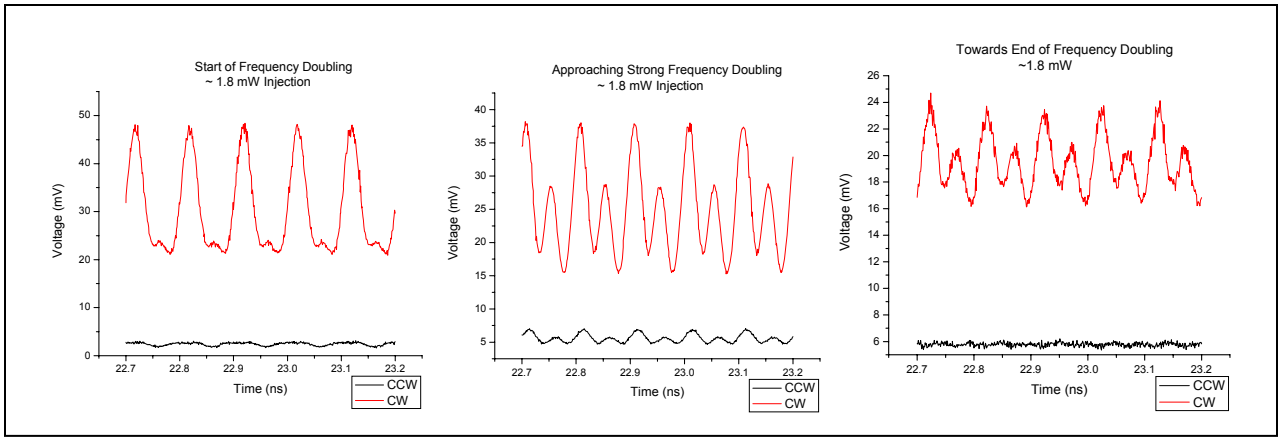

Figure 33. Progression of frequency doubling as an effect of detuning.

4.2.5 Packaged Ring Laser Summary

The amplitude of the co-propagating (CW) mode was always larger than the counter-propagating (CCW) direction. This is most likely explained by the limited amount of carriers, which allows the injected mode to exhibit a dominating effect. Pulsed encoded formats demonstrated digital switching in excess of 10 GHz. Generally, cavity relaxation oscillations limit the response rate for directly modulated diode lasers, but the optically modulated results here indicated that bandwidth limit was enhanced by at least a factor of two. The ring laser consistently exhibited maximum oscillations ~ 4 GHz and is consistent with relaxation effects expectations for this medium and cavity dimension. The extended response was confirmed with single frequency measurements up to 12 GHz. Tests with CW optical injection showed the cavity relaxation rate, i.e. the response bandwidth, could be further enhanced with injected power. This enabled optically modulated operation to nearly 20 GHz in the present laser, and could project to 50 GHz with realistic scaling of the cavity dimensions. The performance discussed here compares with the highest rates achieved in VCSELs and offers a configuration more amenable to integration.

5.0 Theoretical Simulation: Optical Injection Model

Rate equations that model a four port semiconductor ring laser with a modulated optical input signal used for injection locking are presented in this chapter. Numerical simulations were carried out to illustrate the observed "switching" behavior in the intensities of the two circulating modes.

The single mode rate equations that have been used traditionally to model optical injection phenomena in semiconductor lasers consist of three first order nonlinear differential equations, (2)-(4); one for the amplitude of the electric field *R* (photons), the phase difference between the master and slave electrical fields ψ, and the carrier density *N* (electrons):

$$\dot{R} = NR + \eta\cos(\psi) \tag{2}$$

$$\dot{\psi} = \Omega - aN - \frac{\eta}{R}\sin(\psi) \tag{3}$$

$$T\dot{N} = P - N - P(1+2N)R^2 \quad . \tag{4}$$

In this set of equations the time is measured in units of the photon life time of the laser cavity. T is defined as the ratio of the carrier to the photon life times; α is the linewidth enhancement factor, and $\eta$is proportional to the amount of injected light that enters the slave laser cavity and is typically one of the experimentally controlled parameters. P is the pumping electrical current threshold, and it is proportional to:

$$P \sim \frac{J}{J_{th}} - 1, \tag{5}$$

where J and J_{th} denote the pumping current and the pumping current at threshold respectively. Finally Ω denotes the frequency detuning between the master and slave lasers and is also one of the experimentally controlled parameters.

This set of equations can be written in a compact complex form as follows:

$$\dot{\hat{E}} = (1+i\alpha)N\hat{E} + \eta e^{i\Omega t} \tag{6}$$

$$T\dot{N} = P - N - P(1+2N)\left|\hat{E}\right|^2 \quad , \tag{7}$$

where the complex electric field is given by $\hat{E}(t)=R\exp(i\psi)$.

The semiconductor laser is known to be sensitive to external perturbations and can exhibit nonlinear dynamics in its performance due to a combination of strong phase amplitude coupling, relatively high gain per length unit, and relatively long carrier lifetime. The electron carrier lifetime is typically of the order of one nanosecond, compared to a photon round-trip time in the cavity on the order of one picosecond. The most notable dynamical consequence of these factors

is the relaxation oscillation, a damped periodic exchange between the intensity and inversion (number density of the gain medium) of the laser[6,7]. The resulting nonlinear dynamics pose undesired features for many applications, since they affect both the continuous wave and modulated performance of the laser. However, such "instabilities can be domesticated" and can be tailored so as to enable novel practical applications such as bandwidth enhancement and high speed switching.

The key formula for the free running relaxation oscillation is expressed as follows:

$$f_r = \frac{1}{2\pi\tau_p}\sqrt{\frac{2P}{T}}, \tag{8}$$

where τ_p denotes the photon life time of the laser cavity. This can be calculated by performing linear stability analysis on the lasing steady state when the injection level is zero. When η is zero the system becomes effectively two dimensional, and a simple calculation can compute the damping and the free running relaxation oscillation.

The results are given by the following formulas:

$$\gamma_r = \frac{1+2P}{2T} \tag{9}$$

$$\omega_r = \sqrt{\frac{2P}{T} - \gamma_r^{\,2}} \approx \sqrt{\frac{2P}{T}} \quad . \tag{10}$$

To establish connection with the more traditional formulation given in most IEEE journals and semiconductor texts, the following section includes a discussion of various transformations needed to bring the set of evolution equations into that compact form.

5.1 Equation Transformations

The semiconductor rate equations consist of two ordinary differential equations, one for the complex electric field mode, and one for the carrier number N. They are given as follows [8- 11, 13]:

$$\frac{d\mathrm{E}}{dt} = \frac{1}{2}[G_n\Gamma(1+i\alpha)(N-N_t) - \frac{1}{\tau_p}]\mathrm{E} - i(\omega_2-\omega_1)\mathrm{E} - \mathrm{E}_{ext} \tag{11}$$

$$\frac{dN}{dt} = \frac{J}{q} - \frac{N}{\tau_s} - G_n(N-N_t)\left|\mathrm{E}\right|^2 \tag{12}$$

where G_n is the differential gain; Γ is the confinement factor; N_t is the transparency carrier number; τ_p is the photon life time; E_{ext} is the incident electrical field amplitude; I=J is the electrical injection current; q is the elementary charge, and τ_s is the carrier lifetime. The

difference $\omega_2 - \omega_1$ is defined as the detuning between the injected and the time-dependent laser frequency. It is given by

$$\omega_2 - \omega_1 = \Delta\omega_o - \frac{1}{2}\alpha G_n \Gamma (N - N_o) \quad , \tag{13}$$

where $\Delta\omega_o$ is the fixed optical detuning between the frequencies of the external field and the free running slave laser; α is the linewidth enhancement factor, and N_o is the steady state carrier number at zero injection. This implies that

$$\frac{d\mathrm{E}}{dt} = \frac{1}{2}[G_n \Gamma (1 + i\alpha)(N - N_{th})]E - i\Delta\omega_o \mathrm{E} - \mathrm{E}_{ext} \tag{14}$$

$$\frac{dN}{dt} = \frac{I}{q} - \frac{N}{\tau_s} - [G_n (N - N_{th}) + \frac{1}{\Gamma \tau_p}]|\mathrm{E}|^2 \quad . \tag{15}$$

The following dimensionless variables and parameters are introduced as follows:

$$Eletric\ field\ \ Y \equiv \sqrt{\frac{\tau_s G_n}{2}} E \tag{16}$$

$$Number\ \ density\ \ Z \equiv \frac{\tau_p G_n \Gamma}{2}(N - N_{th}) \tag{17}$$

$$Dimensionless\ time,\ s \equiv \frac{t}{\tau_p} \quad . \tag{18}$$

So the set of equations acquires the following compact form:

$$\frac{dY}{ds} = (1 + i\alpha)ZY + i\Omega Y + \mu \tag{19}$$

$$T\frac{dZ}{ds} = P - Z - (1 + 2Z)|Y|^2 \quad . \tag{20}$$

Introducing the variables R and ψ and the parameters,

$$\eta = \mu / \sqrt{P} \tag{21}$$

$$Y = \sqrt{P}\,\mathrm{Re}\,xp(i\psi) \quad , \tag{22}$$

the original equations are obtained.

All the relevant parameters are, therefore, defined as follows:

$$\mu = -\tau_p \sqrt{\frac{\tau_s G_n}{2}} E_{ext} \tag{23}$$

$$\mathrm{T} \equiv \frac{\tau_s}{\tau_p} \tag{24}$$

$$P \equiv \frac{\tau_p G_n \Gamma N_{th}}{2} \left(\frac{J}{J_{th}} - 1\right) \tag{25}$$

$$J_{th} \equiv \frac{qN_{th}}{\tau_s} \tag{26}$$

$$\Omega \equiv -\Delta\omega_o \tau_p \tag{27}$$

5.2 Optical Injection on Ring Lasers

In the case of a ring shaped diode laser, only single longitudinal mode operation is considered. It is assumed that the other circulating modes are much farther apart in frequency, so their weak mutual interaction does not influence the key features of the overall dynamics. The electric field inside the cavity can be expressed as follows:

$$\mathrm{E}(x,t) = \hat{\mathrm{E}}_1(t)\exp[-i(\omega t - kx)] + \hat{\mathrm{E}}_2(t)\exp[-i(\omega t + kx)] \tag{28}$$

Where $\hat{\mathrm{E}}_1$ and $\hat{\mathrm{E}}_2$ are the slowly varying mean complex electric field amplitudes associated with two propagating directions, i.e. mode 1 (counter clockwise) and mode 2 (clockwise). Parameter 'x' represents the spatial coordinate along the optical path of the ring laser, assumed to be positive in the clockwise direction, while w is the optical frequency associated with the 1550 nm emission wavelength of the selected longitudinal mode.

From these considerations it becomes evident why equations 6 & 7 can be generalized to yield the following rate equation model of the two counter propagating complex electrical fields under optical injection was employed for the simulations:

$$\hat{E}_1 = (1 + i\alpha)N\hat{E}_1 + \eta\exp(i\Omega t) \tag{29}$$

$$\hat{E}_1 = (1 + i\alpha)N\hat{E}_2 \tag{30}$$

$$T\dot{N} = P - N - P(1 + 2N)[|E_1|^2 + |E_2|^2] \tag{31}$$

For notational simplicity E, N, and t are always used with dimensionless units in the equations defined by the transformations.

The explicit time dependence of the injection level introduced by the modulator is expressed as

$$\eta(t) = \eta[1 + m\cos(\Omega_d t)], \tag{32}$$

where η is the unmodulated injection level; m is proportional to the modulation depth, and Ω_d is the modulation frequency measured in terms of the running relaxation frequency ω_r.

5.2.1 Simulations of Traditional Optical Injection (One Mode)

The behavior of a two gain path (two propagating modes) ring laser is not well understood. Before considering the complicated structure, concepts and typical behavior of a traditional externally perturbed semiconductor laser are examined. Some typical results are presented for the dynamics of an optically injected laser in its simplest case, when the optical detuning between the slave and master is zero.

Considering an electrically pumped laser operating above threshold and acting as a slave to the injection laser, the most direct way to describe the dynamics is to compute the electric field, or the intensity, as a function of time. The integration time should be long enough, a few hundred photon lifetimes, to give one potential solution that is well separated from any instability points, such as Hopf bifurcations or period doubling bifurcation points. This ensures various transients have settled and the laser system has reached a stable state. The integration in such dynamical systems is typically accomplished with a fourth order Runge Kutta algorithm.

Optical detuning and injection level variation provide two experimental parameters with which to map out stable and unstable regions. The transformed equations, with the fast time scale removed, are much less cumbersome, since everything is then measured in terms the system's free running relaxation oscillation. The "time" in the computational experiments becomes

$$z(time) = \sqrt{\frac{2P}{T}}t \quad . \tag{33}$$

Inspection of the formula shows that the parameter T plays a critical role in the dynamics of these systems. All known and previously investigated semiconductor laser gain structures had very large values (T ~ 1000), which stems from the fact that circulating photons have much shorter transit times (~ picoseconds), compared with much slower electrons (nanoseconds).

Rather than recording all of the time based computations as key parameters are altered, it is customary to display only the extrema, the minimum and the maximum. With this representation the well known continuous wave operation of a laser is nothing else but a single point solution. A typical periodic solution having one frequency is represented by two points, one minimum and one maximum, and therefore, a typical period doubling solution has four points. Chaotic solutions are represented by a random scattering of points. For continuity in these fairly massive

computations, the output condition is used as an initial condition for the following computation, thus generating hysteretic phenomena or coexisting solutions (attractors).

Examining a bifurcation plot helps to distinguish chaos from quasi-periodicity, a periodic solution which has two well separated frequencies. Figure 34 depicts this well known scenario[10, 11,13]. The y-axis represents the deviation of the steady state amplitude of the electric field (R=1+a, which must be kept distinct from the notation for the linewidth enhancement factor α), versus the strength of optical injection electric field, η. For a continuous wave laser, steady state behavior exists from zero injection up to ~0.003 indicated by the flat line. A limit cycle follows where the intensity is periodic and, thus, purely harmonic. This is experimentally verified by examining the radio frequency spectrum, which will consist of side bands separated by the frequency of the limit cycle, i.e. the free running relaxation oscillator. If an optical spectrum analyzer has sufficient resolution, optical spectrum side bands can be viewed as in Figure 31. Period doubling is depicted in Figure 34 in the range ~$0.0095 < \eta < 0.0105$, and the random points in the range $\eta > 0.0105$ suggests that the slave laser entered the region of chaos, i.e. coherence collapse.

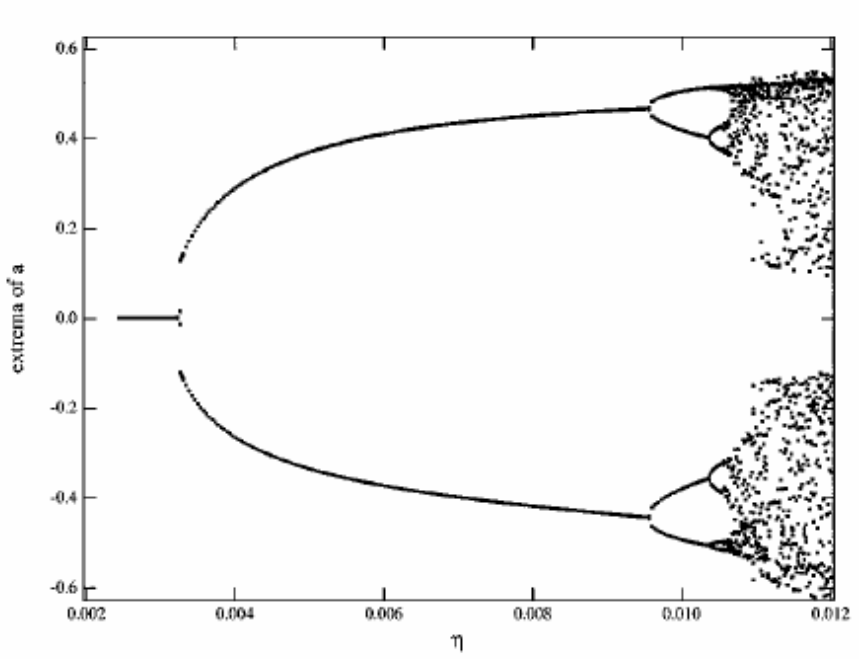

Figure 34. Exemplary bifurcation diagram[10,11,13] for a traditional (single gain path) optically injected laser diode. The y-axis measures the deviation of the steady state amplitude of the electric field R=1+a. The x-axis measures the strength of optical injection electric field. For CW operation the steady state, limit cycle, period doubling and chaotic solutions are depicted.

5.2.2 Hopf Bifurcation

In bifurcation theory (quantitative theory of nonlinear differential equations), a Hopf bifurcation is a local bifurcation in which a fixed point representing a steady state for CW operation loses stability. This is represented as pairs of complex conjugate Eigen values of the linearization around the fixed point, whose locus crosses the imaginary axis of the complex plane. Under reasonably generic assumptions about the dynamical system, a small amplitude limit is expected to cycle and branch from the fixed point. The limit cycle is orbitally stable if a certain quantity, called the first Lyapunov coefficient, is negative, and the bifurcation is supercritical. Otherwise the system is unstable, and the bifurcation is subcritical, hysteretic[12].

5.2.3 Dynamics of Diamond Shaped Lasers

Presented here are numerical simulations of an optically injected diamond shaped laser, modeled as a system of two coupled rate equations as described in the previous section. Figure 35 illustrates how the extrema of the two counter propagating modes take shape as the amount of injection level increases. The diagram shows how the laser transitions from a steady state solution through a Hopf bifurcation and enters into a limit cycle, indicating that the relaxation oscillation has been undamped.

For the numerical computations, parameters were judiciously chosen (i.e. close to those of prior numerical studies): α=5, T=155, P=1.2, with detuning $\Omega=0.1\Omega_R$, recalling the experiments measured approximately 4.5-6.0 GHz for the free running relaxation oscillation of the ring laser. The modulation depth was m = 1, and the modulation frequency ranged from 0.1 to 1.1 Ω_R.

Experimentally, once the laser was injection locked with side modes substantially suppressed, it was found that as the strength of the injection was increased, the common steady state (CW operation) split such that the injected mode typically obtained most of the energy. Literature agrees with this injection phenomenon and suggests that increasing the injection level further yields various well known instabilities, including undamping of the free running relaxation oscillations across a Hopf bifurcation, period doubling and chaotic emission[13].

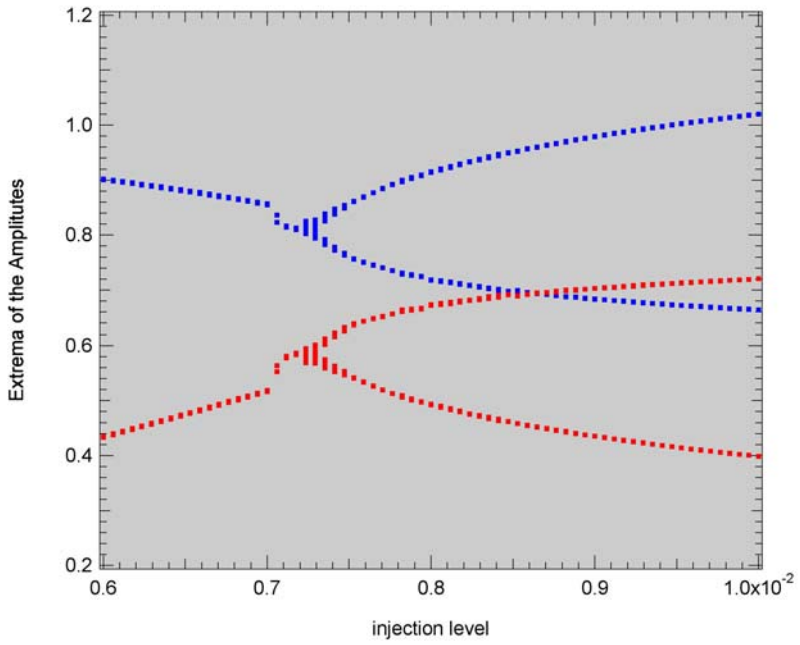

Figure 35. Typical bifurcation diagram showing the minima of the two counter propagating intensities as the level of injection changes.

In Figure 36 the two counter propagating mode intensities oscillate about the continuous wave steady states denoted by horizontal lines at injection level 0.76 and 0.22. A key observation is that the intensities are anti-correlated suggesting that this level of optical modulation tends to switch the output light of the two counter propagating electric fields. From this set of simulations it is clear that a simplified model, which does not include nonlinear gain and optical coupling between the two modes, is able to capture certain key qualitative characteristics of the dynamic response of the Binoptics diamond ring laser configuration.

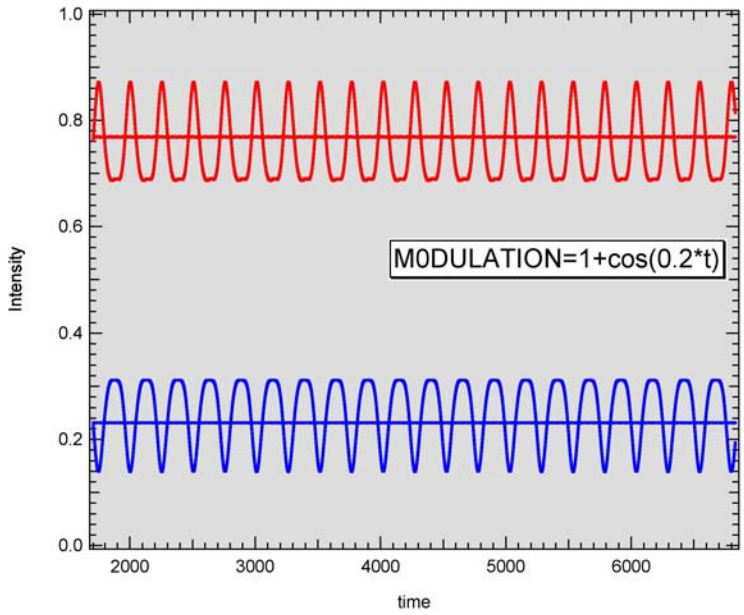

Figure 36. Time evolution of the two intensities as a function of dimensionless time as defined in the text. Switching behavior with clearly anti correlated intensities is observed at injection level 0.0067 and modulation depth m=1. The horizontal lines denote the CW operation with unmodulated optical injection.

Qualitative agreement between the above simulations and the measured experimental dynamical responses are further depicted in Figures 37.

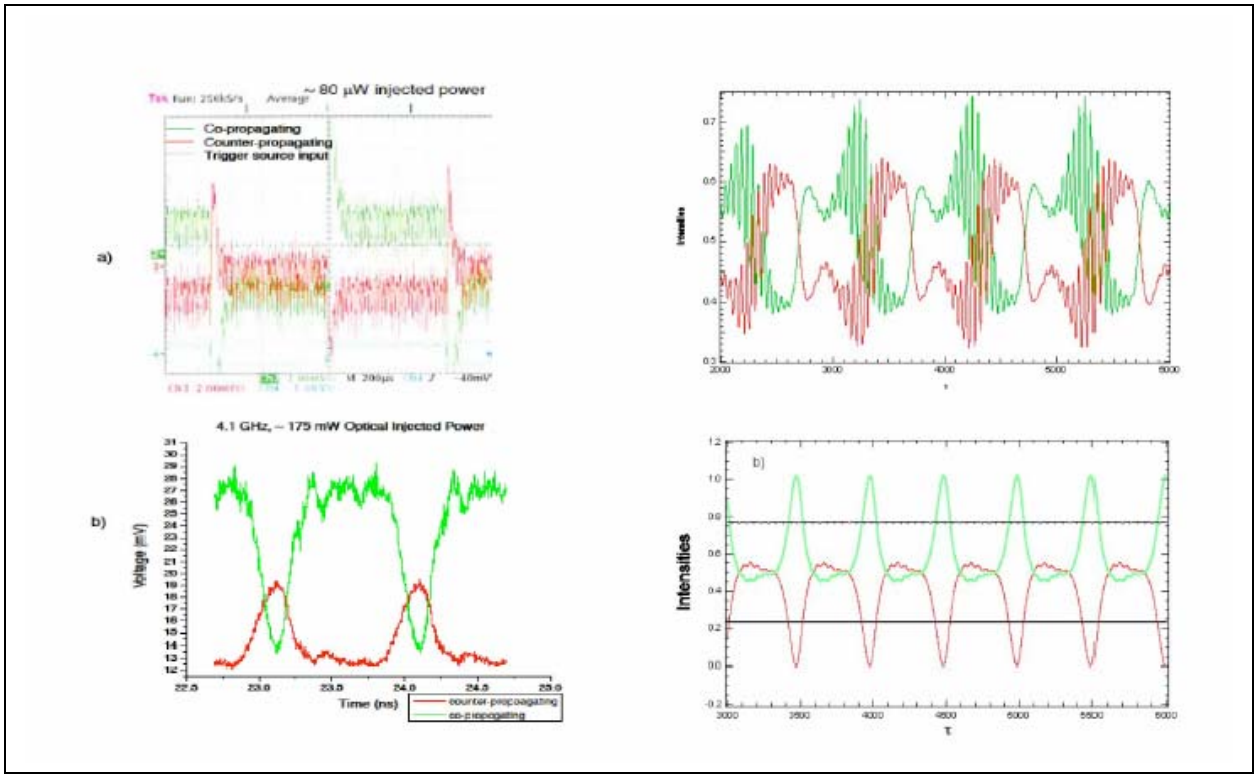

Figure 37. (Left) Representative experimental results of co- and counter-propagating modes for optically modulated injection at (a) 700 Hz and (b) 4.1 with a 1 on-3 off negative logic format. (Right) Theoretical results of co- and counter-propagating modes for (a) 1% of the relaxation running oscillation frequency and (b) just below free running relaxation oscillation frequency.

At slow driving frequency, ~ 1% of Ω_r, Figure 37a depicts the response waveforms of the intensities, which consist of the fast relaxation oscillations modulated within the slow envelope of the driving frequency. In the region where the driving frequency is close to, but just less than, Ω_r, shown in Figure 37b, anti-correlated intensities between the two modes indicate the presence of the switching phenomena.

The results from the presented model showed good qualitative agreement with measured data for both slow modulation speeds, ~ 700 MHz, and high speeds, on the order of the free running relaxation oscillation ~ 4-6 GHz for the diamond shaped ring laser. It is somewhat remarkable that there was no need to include optical coupling or nonlinear gain in order to achieve a degree of qualitative agreement over a large frequency span. Those inclusions in a more comprehensive model may, however, still be required to account for the additional experimental observations that the switching phenomena was observed at discreet values of detuning, rather than at zero detuning.

6. Conclusions

Four-port fiber coupled ring lasers, to the best of our knowledge, not been previously assembled or tested. The design having two coupled optical gain paths in a semiconductor medium, with four-port interactive optical access, offers unprecedented degrees of freedom for optical control. The packaged devices allowed systematic testing of bandwidth limitations. The large parameter space also presents new challenges to the complex analysis of the device physics.

This work successfully addressed several related questions of fundamental importance:

1) Under what conditions could the unique switching effect in these semiconductor ring laser devices be applied in actual practice as an optical comparator or switch/router for digital optical logic?

2) Does the performance in terms of threshold power and frequency range offer significant advantage over present state-of-the-art electronic technology?

3) Can the theoretical understanding of injection locked semiconductor lasers be generalized to include this more complex dual cavity configuration? In particular, how can the switching effects be quantitatively modeled so as to exhibit the relative contribution of both carrier density changes and stimulated photon effects?

Very practical optically switched extinction ratios of ~ 9 dB were observed, and that value could be increased with higher injected power. Optimum switching occurred when the wavelength was detuned, or offset, to match the injected modulation frequency. Pulse encoded data yielded some lower frequency effects which may be attributed to residual reflections in the system, but also exhibited oscillations between 4 and 6 GHz, consistent with relaxation oscillations in the expected range for this medium and cavity dimension. This effect was not as evident for single frequency input signals, which is most likely due to their much smaller perturbation to the steady state compared with a square waveform.

No response is expected when the drive current of a diode laser is directly modulated beyond its relaxation frequency, so the observations at twice that value with time-varying optical injection indicate a contribution to switching effects by photon stimulation. However, the observed cutoff at about 15 GHz could imply that the relaxation effects still play a limiting role, and that a combined effect is at work. Conclusions must at this point be guarded until more complete tests are done with sufficient cavity variation to alter and isolate the contribution of the relaxation oscillation. These methods have been successfully demonstrated at Binoptics in Fabry-Perot semiconductor diode lasers, but not in this significantly more complex configuration. A theoretical model shows that with proper conditions the laser mode intensities are expected to be anti-correlated with laser injection, as we observed.

The remarkable development of these unique semiconductor ring laser devices was initially motivated by the need for an ultra high speed optical comparator in the A/D converter effort pursued at SNDP. The packaged prototypes successfully demonstrated the key performance

specifications; the response rates exceeded 10 GHz rates and could be projected up to 50 GHz with modification to already proven technology. The limits to scaling of the channel number still remain to be determined by future work.

The new device physics of this semiconductor ring laser is of fundamental interest to understanding of electro-optical effects of interacting control signals in a semiconductor medium. These investigations broadened the scope of applications to include the high speed optical logic functions as originally envisioned by Grande and Tang[14] and currently pursued in recent polarization switched VCELS[2].

As far as we are aware, the devices characterized in this work have demonstrated higher frequency performance than any existing devices offering comparable integrated multi-port access. The results of this research were accordingly presented in several relevant military symposia and engineering conferences to promote awareness of this newly developed technology[5,15-17].

References

1. Rebecca Bussjager, Michael Hayduk, Steven Johns, Michael Fanto, Reinhard Erdmann, Joseph Osman, John Malowicki and David Winter, "*Photonic Analog-to-Digital Converters," AFRL-SN-RS-TR-2006-109*, Mar. 2006.

2. Sylvain Barbay, Giovanni Giacomelli, and Francesco Marin, "Stochastic Resonance in Vertical Cavity Surface Emitting Lasers," *Phys. Rev.* E, Vol. 61, pp. 157-166, 2000.

3. See Binoptics Website: www.binoptics.com.

4. Malcolm Green, "Optical Injection and Switching Using Diamond Shaped Semiconductor Ring Lasers for Analog to Digital Photonic Converters," *AFRL-SN-RS-TR-2003-308*, Jan. 2004.

5. Nancy Stoffel, Songsheng Tan, Charles Shick, Wesley Bacon, Bryan Beaman, Alan Morrow, Malcolm Green, Rebecca Bussjager, Steve Johns, Michael Hayduk, Joseph Osman, Reinhard Erdmann, and Brian McKeon, "Diamond Shaped Ring Laser Characterization, Package Design and Performance," *56th Electronic Components and Technology Conference Proceedings*, pp. 1583-1589, June 2006.

6. K. Petermann, *Laser Diode Modulation and Noise* (Springer-Verlag, Berlin, 1991).

7. *Unlocking Dynamical Diversity: Optical Feedback Effects on Semiconductor Lasers*, edited by D. M. Kane and K. A. Shore (Wiley, New York, 2005).

8. Roy Lang, "Injection Locking Properties of a Semiconductor Laser," *IEEE J. of Quantum Electronics,* Vol. 18, No. 6, 976-983, June 1982.

9. G. H. M. Van Tartwijk, H. de Waardt, B. H. Verbeek and D. Lenstra, "Resonant Optical Amplification in a Laser Diode: Theory and Experiment," *IEEE J. of Quantum Electronics, Vol.* 30**,** No. 8, p.1763, August 1994.

10. T. B. Simpson, J.M. Liu, A. Gavrielides, V. Kovanis and P.M. Alsing, "Period-Doubling Route to Chaos in a Semiconductor Laser Subject to Optical Injection," *Applied Physics Letters*, pp. 3539-3541, 1994.

11. T. B. Simpson, J.M. Liu, A. Gavrielides, V. Kovanis and P.M. Alsing, "Period-Doubling Cascades and Chaos in a Semiconductor Laser with Optical Injection," *Physical Review A*, Vol. 51, pp. 4181-4185, 1995.

12. Steven H. Strogatz, *Nonlinear Dynamics and Chaos* (Addison Wesley, 1994).

13. V. Kovanis, A. Gavrielides, T. B. Simpson, and J. M. Liu, "Instabilities and Chaos in Optically Injected Semiconductor Lasers," *Applied Physics Letters*, Vol. 67, pp. 2780-2782, 1995.

14. W. J. Grande and C. L. Tang, "Semiconductor Laser Logic Gate Suitable for Monolithic Integration," *Applied Physics Letters*, Vol. 51, pp. 1780-1782, 1987.

15. Rebecca Bussjager, Reinhard Erdmann, Vassilios Kovanis, Brian McKeon, Steven Johns, Alan Morrow, Malcolm Green, Nancy Stoffel, Songsheng Tan, Charles Shick, Wesley Bacon, Bryan Beaman," Packaged Diamond-Shaped Ring-Laser Diode Switch," *2006 IEEE AVFOP Proceedings*, pp. 64-65, Sep. 2006.

16. Vassilios Kovanis, Reinhard Erdmann, Rebecca Bussjager, Brian McKeon, Steven Johns, Alan Morrow, Malcolm Green, Nancy Stoffel, Songsheng Tan, Charles Shick, "Optical Modulation of Diode Ring Lasers," Post deadline paper to *2006 IEEE LEOS Annual Meeting Proceedings*, Oct. 2006.

17. Rebecca Bussjager, Reinhard Erdmann, Vassillios Kovanis, Brian McKeon, Michael Fanto, Steve Johns, Michael Hayduk, Joseph Osman, Alan Morrow, Malcolm Green, Nancy Stoffel, Songsheng Tan, Charles Shick, Wesley Bacon, Bryan Beaman, "Injection Characterization of Packaged Bi-Directional Diamond Shaped Ring Lasers at 1550 nm," *SPIE Proceedings: Enabling Photonics Technologies for Defense, Security and Aerospace Applications II,* Vol. 6243, Jul. 2006.